Human Molecular Genetics, 2018, Vol. 0, No. 0 1–19

doi: 10.1093/hmg/ddy059
Advance Access Publication Date: 14 February 2018
Original Article

ORIGINAL ARTICLE

Alpha-synuclein inhibits Snx3–retromer-mediated retrograde recycling of iron transporters in *S. cerevisiae* and *C. elegans* models of Parkinson's disease

Dhaval Patel[1], Chuan Xu[2], Sureshbabu Nagarajan[1], Zhengchang Liu[3], Wayne O. Hemphill[1], Runhua Shi[4], Vladimir N. Uversky[5], Guy A. Caldwell[2], Kim A. Caldwell[2] and Stephan N. Witt[1,6,*]

[1]Department of Biochemistry and Molecular Biology, Louisiana State University Health Sciences Center, Shreveport, LA 71130, USA, [2]Department of Biological Sciences, The University of Alabama, Tuscaloosa, AL 35487, USA, [3]Department of Biological Sciences, The University of New Orleans, New Orleans, LA 70148, USA, [4]Department of Medicine, Feist-Weiller Cancer Center, Louisiana State University Health Sciences Center, Shreveport, LA 71130, USA, [5]Department of Molecular Medicine, USF Health Byrd Alzheimer's Research Institute, Morsani College of Medicine, University of South Florida, Tampa, FL 33612, USA and [6]Pharmacology, Toxicology and Neuroscience, Louisiana State University Health Sciences Center, Shreveport, LA 71130, USA

*To whom correspondence should be addressed at: Department of Biochemistry and Molecular Biology, Louisiana State University Health Sciences Center, 1501 Kings Highway, Shreveport, LA 71130, USA. Tel: +1 3186755163; Fax: +1 3186755180; Email: switt1@lsuhsc.edu

Abstract

We probed the role of alpha-synuclein (α-syn) in modulating sorting nexin 3 (Snx3)-retromer-mediated recycling of iron transporters in *Saccharomyces cerevisiae* and *Caenorhabditis elegans*. In yeast, the membrane-bound heterodimer Fet3/Ftr1 is the high affinity iron importer. Fet3 is a membrane-bound multicopper ferroxidase, whose ferroxidase domain is orthologous to human ceruloplasmin (Cp), that oxidizes external Fe^{+2} to Fe^{+3}; the Fe^{+3} ions then channel through the Ftr1 permease into the cell. When the concentration of external iron is low (<1 μM), Fet3/Ftr1 is maintained on the plasma membrane by retrograde endocytic-recycling; whereas, when the concentration of external iron is high (>10 μM), Fet3/Ftr1 is endocytosed and shunted to the vacuole for degradation. We discovered that α-syn expression phenocopies the high iron condition: under the low iron condition (<1 μM), α-syn inhibits Snx3–retromer-mediated recycling of Fet3/Ftr1 and instead shunts Fet3/Ftr1 into the multivesicular body pathway to the vacuole. α-Syn inhibits recycling by blocking the association of Snx3-mCherry molecules with endocytic vesicles, possibly by interfering with the binding of Snx3 to phosphatidylinositol-3-monophosphate. In *C. elegans*, transgenic worms expressing α-syn exhibit an age-dependent degeneration of dopaminergic neurons that is partially rescued by the iron chelator desferoxamine. This implies that α-syn-expressing dopaminergic neurons are susceptible to changes in iron neurotoxicity with age, whereby excess iron enhances α-syn-induced neurodegeneration. *In vivo* genetic analysis indicates that α-syn dysregulates iron homeostasis in worm dopaminergic neurons, possibly by inhibiting SNX-3-mediated recycling of a membrane-bound ortholog of Cp (F21D5.3), the iron exporter ferroportin (FPN1.1), or both.

Received: December 1, 2017. **Revised:** February 7, 2018. **Accepted:** February 12, 2018

Introduction

Parkinson's disease (PD) is defined by the progressive degeneration of dopaminergic neurons in the mid-brain region called the *substantia nigra par compacta* (SNpc) (1). Loss of these neurons leads to resting tremor, slowness of movement and disturbances in gait and balance. Surviving neurons often contain cytoplasmic proteinaceous inclusions called Lewy bodies, the principal component of which is the protein α-syn (2,3). Wild-type α-syn has been implicated in sporadic PD; whereas, missense mutations (4–8) or multiplications of the α-syn gene cause early-onset PD (9).

α-Syn, which is highly expressed in dopaminergic neurons, has been suggested to be a lipid carrier (10), a regulator of synaptic vesicle fusion with the presynaptic membrane (11), and a protein involved in iron metabolism (12). The focus of this study is the role of α-syn in iron metabolism, specifically, the mechanism by which α-syn alters the retrograde endocytic trafficking of iron transporters.

The total iron increases in the SNpc in severe cases of PD (13–15), and biochemical studies have demonstrated a mechanistic link between iron accumulation and α-syn toxicity. Neurotoxin based animal models of PD have shown that intracellular iron increases with loss of striatal dopamine (DA), and this increased iron likely contributes to cell death (16–20). These findings have led to the hypothesis that excess iron initiates dopaminergic neurodegeneration in PD, although the mechanism by which this occurs remains elusive.

The interplay between α-syn homeostasis and iron homeostasis was modeled herein using yeast and nematodes. Eukaryotes have a tightly regulated network of proteins that import, export, and store iron. Yeast cells can import and store but not export iron. Yeast rapidly responds to changes in the level of environmental iron, and here we are interested in the case of low external iron. Low external iron activates the transcription of four genes—*FET3*, *FTR1*, *FRE1* and *FRE2*—involved in the acquisition of iron (21,22). Three of these four membrane-bound proteins (Fet3, Fre1 and Fre2) have their enzymatic domains on the exofacial side of the plasma membrane. Fet3/Ftr1 is the high affinity iron import complex, whereby Fet3 functions as a multicopper ferroxidase and Ftr1 is a ferric iron permease. These two proteins form a complex in the endoplasmic reticulum, which then transits through the secretory pathway to the plasma membrane. Fre1 and Fre2 are metalloreductases that reduce environmental Fe^{+3} to Fe^{+2}. The labile Fe^{+2} ions are captured by Fet3, re-oxidized, and then transported into the cell by Ftr1 (23,24) (Fig. 1A). Humans express two orthologs of Fet3, i.e. serum ceruloplasmin and hephaestin; a rare glycosylphosphatidylinositol-anchored form of ceruloplamin is expressed in astrocytes (25).

Fet3/Ftr1 complexes are also subject to posttranslational regulation. When the concentration of external iron is low (<1 μM), Fet3/Ftr1 is maintained on the plasma membrane by the endocytic-recycling pathway (Fig. 1B) (26,27). However, when the external iron concentration is high, the number of Fet3/Ftr1 complexes on the plasma membrane is down regulated by internalization, followed by the sorting of Fet3/Ftr1 vesicular cargo to the vacuole for degradation (Fig. 1B).

Endocytosis is an emerging area regarding the etiology of PD because the conserved gene *VPS35*, which encodes a component of the endocytic recycling complex called retromer, is mutated in some cases of late-onset PD (28–30), and overexpression of endocytosis-related genes can rescue α-syn toxicity (31,32). Retromer is a highly conserved multimeric protein complex that orchestrates the sorting, export, and retrieval of cargo proteins from early endosomes (33–35). Composed of five proteins, retromer binds on the cytosolic face of early endosomes (Fig. 1C). One sub-complex of retromer is the Vps26-Vps29-Vps35 trimer (hVps26, hVps29, hVps35 in humans) (36), which is involved in cargo selection. The other sub-complex is the membrane-associated heterodimer Vps5-Vps17 (Snx1 and Snx2 in humans), which is involved in the deformation of the endocytic vesicles into tubules (37,38). The sorting nexins Vps5 and Vps17 each contain two membrane-binding domains: a phox homology (PX) domain that binds preferentially to phosphatidylinositol-3-monophosphate (PI3P) (39), which is enriched in early endosomes, and a BIN/Amphiphysin/Rvs (BAR) domain that senses membrane curvature and remodels endosomes into tubules (40). For cargo to be retrieved from the degradative pathway, this multimeric retromer complex must bind to the sorting signal sequence on the cargo in early endosomes. This is followed by the formation of endosomal tubules from which retromer-cargo vesicles bud off and then transit to the trans-Golgi for recycling to the plasma membrane (41).

Retromer-mediated recycling of Fet3/Ftr1 (42–44) has been studied in detail in yeast (26,27). Retromer, the sorting nexin Grd19/Snx3, and the Golgi Rab GTPase Ypt6 maintain Fet3/Ftr1 on the plasma membrane in the low iron condition (26). The C-terminus of Ftr1 contains an endocytic recycling sequence that specifically binds to Snx3 (26) (Fig. 1C). The Snx3 sorting nexin contains only a PX domain. Recycling occurs after Fet3/Ftr1 is internalized into early endosomes, and upon the binding of Snx3 to the C-terminus of Ftr1, the Snx3-Ftr1/Fet3 complex assembles on the surface of an early endosome with the two retromer subcomplexes Vps26-Vps29-Vps35 and Vps5-Vps17 (Fig. 1C). Formation of this complex causes tubulation, and vesicles bud off from the tubules and transit to the trans-Golgi for transport to the plasma membrane. For iron shocked cells, Fet3/Ftr1 molecules are also internalized, but instead of recycling they are shunted to the vacuole (45).

We report here that α-syn alters the trafficking of Fet3/Ftr1. α-Syn partially blocks the Snx3–retromer-mediated recycling of Fet3/Ftr1, which results in the iron import complex entering the degradative pathway. α-Syn inhibits recycling by blocking the association of Snx3 and Vps17 with early endosomes. We also show that knocking down the worm ortholog of *SNX3*, *snx-3*, has no effect on dopaminergic neurons lacking α-syn expression, whereas knocking down *snx-3* in DA neurons that express α-syn causes severe neurodegeneration, and this neurodegeneration is rescued by an iron chelator. This study raises the possibility that α-syn causes the mistrafficking of iron transporters and thus perturbs iron homeostasis.

Results

Figure 1C shows the proteins involved in the endocytic recycling of Fet3/Ftr1 complexes in yeast. Given that α-syn avidly binds to lipids, membranes and vesicles (46), we asked whether α-syn might interfere with the binding of Snx3 and other retromer components to the surface of endosomes. Such interference by α-syn would alter the endocytic recycling of Fet3/Ftr1 complexes. A strain called TSY145 (Table 1), which expresses Snx3-mCherry and modified forms of both Fet3 and Ftr1 in which lysine residues facing the cytoplasm are replaced with arginine, was used for these experiments. The Fet3–(4K/R)-HA/Ftr1–(18K/

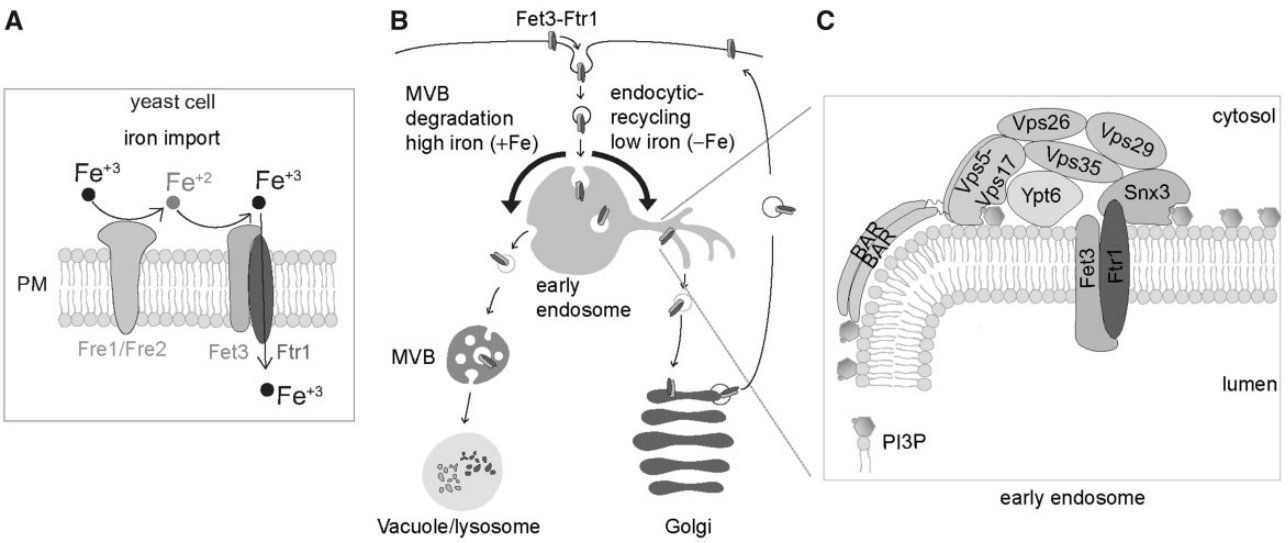

Figure 1. Illustration of iron import and endocytic recycling of iron import proteins in yeast. (**A**) The ferric reductases Fre1 and Fre2 reduce environmental iron ($e^- + Fe^{+3} \rightarrow Fe^{+2}$). Fet3 then oxidizes Fe^{+2} ions to Fe^{+3} ions, and in concert the Fe^{+3} ions channel through the Ftr1 permease into the cytosol. This oxidation step is coupled to the passage through Ftr1. (**B**) Endocytic recycling. The iron import proteins Fet3/Ftr1, which have a high-affinity for iron, are expressed in response to low external iron, and the complexes are maintained on the plasma membrane by endocytic recycling between the plasma membrane and Golgi. If the external iron concentration increases above 10 μM, Fet3/Ftr1 complexes are endocytosed and shunted into the MVB pathway, which delivers the proteins to the vacuole for degradation. (**C**) Snx3–retromer binds to Fet3/Ftr1. Snx3 is a cargo-specific adaptor protein that specifically binds to the endocytic recycling sequence on the C-terminus of Ftr1. Vps26-Vps29-Vps35 is the retromer cargo recognition complex. Vps5-Vps17 is the membrane recognition complex. Snx3 is a cargo-specific adapter protein that binds to the C-terminus of Ftr1.

Table 1. Yeast strains and plasmids

Strains	Genotype	Source or reference
Wild-type	BY4741/*MATa his3Δ1 leu2Δ0 met15Δ0 ura3Δ0*	Open Biosystems
Fet3-GFP	BY4741/*FET3-GFP:: HIS3MX*	Life Technologies
Ftr1-GFP	BY4741/*FTR1-GFP:: HIS3MX*	Life Technologies
Vac1-GFP	BY4741/*VAC1-GFP:: HIS3MX*	Life Technologies
Fet3-GFP-*pep4Δ*	Fet3-GFP/*pep4Δ:: KANMX4-2*	Zhengchang Liu
TSY143	BY4742/*MATα his3Δ leu2Δ0 lys2Δ0 ura3Δ0; FET3(4K/R)-3HA:: HISMX; FTR1(18K/R)-GFP:: NATMX; VPS17-mCherry:: KANMX*	Chris G. Burd
TSY145	BY4742/*MATα his3Δ1 leu2Δ0 lys2Δ0 ura3Δ0; FET3(4K/R)-3HA:: HISMX; FTR1(18K/R)-GFP:: NATMX; SNX3-mCherry:: KANMX*	Chris G. Burd
fet3Δ	BY4741/*FET3Δ:: KANMX6*	Open biosystems
ftr1Δ	BY4741/*FTR1Δ:: KANMX6*	Open biosystems
Plasmids	Description	Source
pAG426GAL	2 μ, *URA3*, P_{GAL1}	Addgene
pAG426-α-Syn	pAG426GAL, P_{GAL1}-α-Syn	(90)
pTS22	Plasmid harboring yeast *SNX3*	Chris G. Burd

R)-GFP (lysineless Fet3/Ftr1) mutant complex cannot be ubiquitylated and, therefore, fails to enter the multivesicular body (MVB) pathway. This strain tends to exhibit higher levels of Snx3-mCherry fluorescence on endosomes. The validation/characterization of the TSY145 strain and *FET3* and *FTR1* deletion strains are shown in Supplementary Material, Figure S1A–D.

α-Syn decreases the number of Snx3-mCherry and Vps17-mCherry puncta. Figure 2A shows that 63% of empty vector (EV) control cells exhibited red puncta. Such puncta are endosomes decorated with Snx3-mCherry. Strikingly, α-syn decreased the percentage of cells exhibiting red puncta; specifically, the percentage of cells decreased from 63% (EV) to 6.9% (α-syn) ($P < 0.0001$) (Fig. 2B). The mean fluorescence intensity of individual red puncta in α-syn cells was even significantly less than in EV cells (Fig. 2C; $P = 0.0221$). Western blotting showed that α-syn failed to change the expression level of Snx3-mCherry (Fig. 2D and E). The results suggest that α-syn disrupts the binding of Snx3-mCherry to the surface of early endosomes.

To ascertain whether α-syn affects the endosomal localization of the retromer heterodimer composed of Vps5-Vps17, each of which has a PX and BAR domain (Fig. 1C), we used strain TSY143 (Table 1) which harbors an integrated copy of Vps17-mCherry. α-Syn indeed significantly decreased the percentage of cells exhibiting red puncta (Fig. 2F and G), but it did not decrease the level of the Vps17-mCherry protein (Fig. 2H and I). Collectively, the results show that α-syn significantly decreases

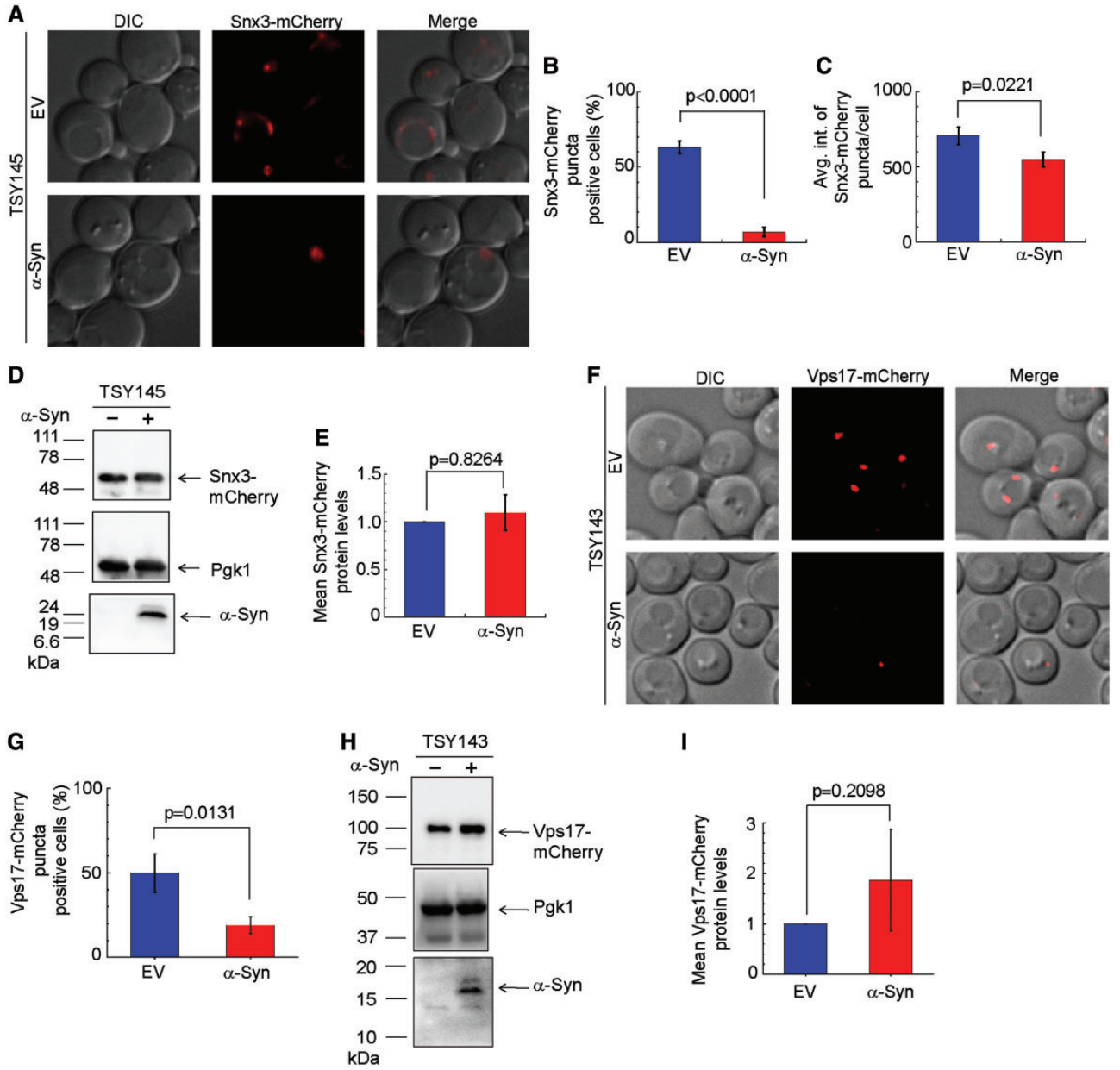

Figure 2. α-Syn disrupts the endosomal localization of Snx3 and Vps17. (**A**) The TSY145 strain transformed with the indicated plasmids was pre-grown overnight in non-inducing media containing 2% glucose, diluted into the same media with 20 μM BPS and cultured for 6 h, after which the cells were spun down and re-suspended in inducing media containing 20 μM BPS and grown for 4 h. Cells were imaged using fluorescence microscopy. One image of Z series is shown. (**B**) Plot of percentage of cells positive for Snx3-mCherry puncta from panel (A). Values are mean ± SD of three independent colonies. ***P = 0.0001 determined by a Student's *t*-test. (**C**) Plot of mean fluorescence intensity of Snx3-mCherry puncta. Values are mean ± SD of three independent colonies. **P = 0.0221 determined by a Student's *t*-test. (**D**) α-Syn does not alter the expression of Snx3-mCherry. Cells were cultured as described in (A). Lysates were subjected to SDS-PAGE followed by western blotting. Pgk1 is the loading control. (**E**) Plot of normalized Snx3-mCherry protein level. Values are means ± SD of three independent colonies. NS, non-significant determined by a Student's *t*-test. (**F**) The TSY143 strain was transformed with indicated plasmids and cultured as described in panel (A). The only difference is the time duration for inducing media which is 8 h. Cells were imaged using fluorescence microscopy. (**G**) Plot of percentage of Vps17-mCherry positive cells from panel (F). Values are means ± SD of three independent colonies. **P = 0.0131 determined by one-way ANOVA with a Dunnett *post hoc* test. (**H**) α-Syn does not alter the expression of Vps17-mCherry. Cells were cultured as described in panel (F). Lysates were subjected to SDS-PAGE for western blotting. Pgk1 is the loading control. Owing to the low expression of α-syn in the TSY143 strain, we used Image Lab software to brighten this and only this image. (**I**) Plot of normalized Vps17-mCherry protein level. Values are mean ± SD of three independent colonies. *P* value was determined by one-way ANOVA.

the number of both Snx3-mCherry and Vps17-mCherry puncta compared with control cells.

α-Syn can decrease the number of Snx3-mCherry/Vps17-mCherry puncta by two mechanisms: (i) α-syn might bind to and disperse early endosomes into smaller vesicles, and this dispersal might explain the loss of Snx3-mCherry puncta in cells expressing α-syn. Supporting this idea, α-syn disperses large synthetic liposomes of a certain size and composition into smaller vesicles (47) or (ii) α-syn might inhibit the binding of the PX domain of Snx3 to PI3P. Each of these possibilities was addressed.

α-Syn fails to block the binding of Vac1-GFP to early endosomes. Vac1 binds via a FYVE domain to PI3P embedded in early

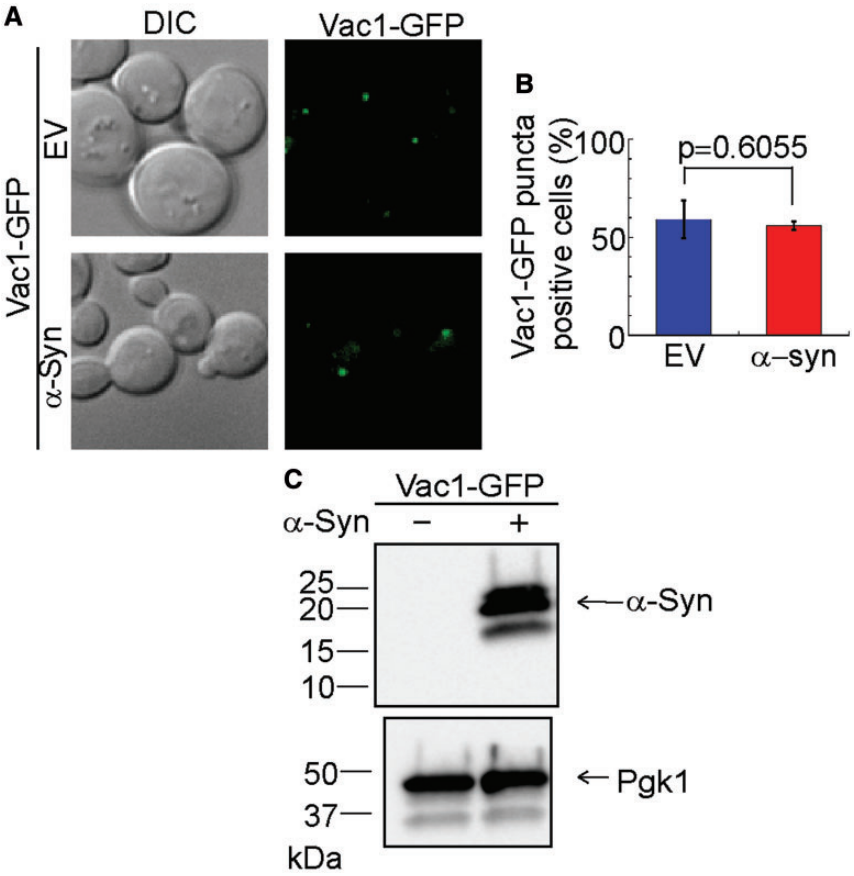

Figure 3. α-Syn does not affect the endosomal localization of Vac1. (**A**) The Vac1-GFP strain transformed with the indicated plasmids was pre-grown overnight in non-inducing media containing 2% glucose, diluted into the same media with 20 μM BPS and cultured for 6 h, after which the cells re-suspended in inducing media containing 20 μM BPS and grown for 4 h. Cells were imaged using fluorescence microscopy. The image is representative of one sub-stack of Z series of images. (**B**) Plot of percentage of cells positive for Vac1-GFP puncta from panel (A). Values are mean ± SD of three independent experiments. About 300 cells were analyzed. The *P* value was determined by a Student's *t*-test. (**C**) α-Syn is expressed in Vac1-GFP strain. Cells were cultured as described in (A). Lysates were subjected to SDS-PAGE followed by western blotting. Pgk1 is the loading control. The intensity of Vac1-GFP signal was relatively weak because there are estimated to be less than 1000 Vac1 molecules per cell; therefore, the brightness (+60) was increased over the entire figure using Adobe Photoshop.

endosomes (48,49). Using a C-terminal fusion of GFP to Vac1, we tested whether α-syn can disrupt the binding of Vac1-GFP to early endosomes. If α-syn functions by mechanism (i), α-syn-expressing cells should have a significantly decreased number of Vac1-GFP foci compared with control cells. However, α-syn had no effect on number of Vac1-GFP foci compared with control cells (Fig. 3A and B). Western blot analysis showed that α-syn was expressed (Fig. 3C). These results indicate that α-syn does not disperse early endosomes.

α-Syn blocks the binding of purified Snx3 to liposomes containing PI3P. Given that Snx3 and Vps17 each contain a PX domain that selectively binds to PI3P, we hypothesized that α-syn blocks the binding of the respective PX domains of Snx3 and Vps17 to PI3P on the surface of early endosomes. Focusing on Snx3, we first verified that purified recombinant yeast Snx3 (Fig. 4A–C) containing a T7 tag binds to PI3P using a PIP strip assay. Snx3 (0.175 μM) bound strongly to PI3P but weakly to phosphatidylinositol-4-phosphate (PI4P), phosphatidylinositol-5-phosphate (PI5P), phosphatidylinositol-3, 5-diphosphate (PI3, 5P2), phosphatidylinositol-4, 5-diphosphate (PI4, 5P2) and phosphatidic acid (PA) (Fig. 4D). Purified recombinant human α-syn was also assessed by western blotting (Fig. 4C). When α-syn was tested in the PIP strip assay, the results were inconclusive because of non-specific binding of α-syn to the strip itself (data not shown).

A flotation assay was used to further test the binding of Snx3 to synthetic liposomes with or without PI3P. The concentration of lipids in solution was 500 μM, and the proportion of lipids was 70%:25%:5% (PC:PS:PI3P or PC:PS:PI). During high-speed centrifugation (200 000*g*) liposomes and liposome-bound proteins migrate to the top of the tube whereas unbound proteins remain in the bottom layer. After the spin, top and bottom fractions were collected and western blotted for Snx3 and α-syn. The flotation assay data were characterized as follows (Fig. 4E and F): (i) Snx3 and α-syn each localized to the bottom of the tube, as expected (lanes 1–4). (ii) α-Syn bound to liposomes with or without PI3P (lanes 8 and 12). (iii) Snx3 bound only to liposomes containing PI3P (compare lanes 10 and 12 to 5 and 7). (iv) α-Syn significantly decreased the percentage (30%) of Snx3 molecules bound to PI3P-containing liposomes compared with control liposomes (compare lanes 11 and 12) (Fig. 4E). These results indicate that α-syn blocks the binding of Snx3 to liposomes containing PI3P.

To test whether α-syn blocks Snx3 binding to PI3P-spiked liposomes in a dose-dependent manner, the concentration of α-syn was varied at a fixed concentration of lipids. Over the α-syn range 1–2.5 μM, there was a linear decrease in the amount

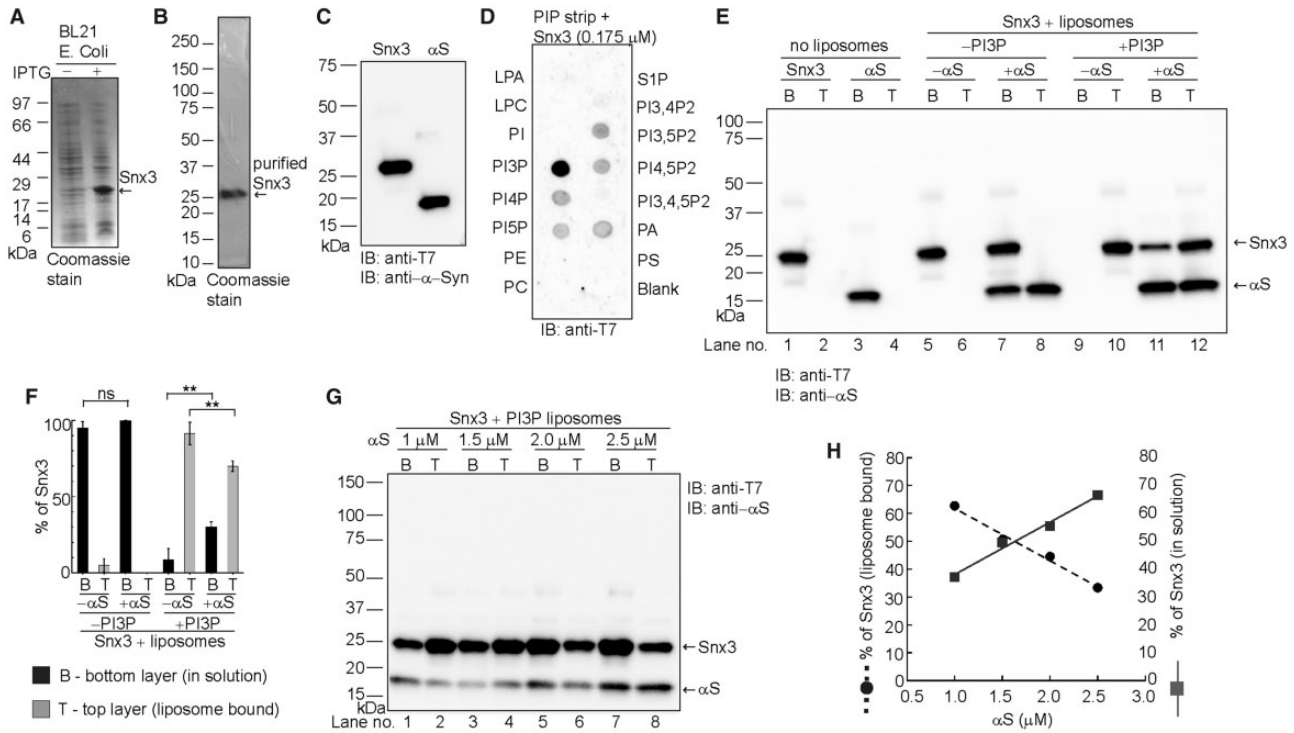

Figure 4. *In vitro* protein-lipid binding assays. (**A, B**) Coomassie blue-stained gels of BL21 (DE3) lysate and purified T7-Snx3. (**C**) Purified recombinant Snx3 and α-syn analyzed by western blotting using monoclonal antibodies against the T7 tag and α-syn. (**D**) PIP strip assay of Snx3 binding. The PIP strip was probed with anti-T7 antibody (1:1000) to detect T7-Snx3. (**E**) Lipid floatation assay showing the membrane bound (T) and free fractions (B) of Snx3 and α-syn analyzed by immunoblotting using monoclonal antibodies against the T7 tag and α-syn. This experiment was conducted three times. (**F**) Plot of mean percent Snx3 for the experiments in panel (E). Snx3 intensities were quantified by ImageJ software and then normalized to the Snx3 intensity in the first lane (Snx3 no liposomes). *P* value (**$P = 0.01$) was determined by a Student's *t*-test. (**G**, E) Lipid floatation assay where the concentration of α-syn was varied at a fixed concentration of lipids. This experiment was conducted three times. (**H**) Plot of mean percent Snx3 from the lipid flotation assay (G).

of liposome-bound Snx3 and a parallel increase in the amount of Snx3 in solution (Fig. 4G and H).

α-Syn decreases the level of the multi-copper ferroxidase Fet3 in exponential-phase cells. Given that α-syn drives Snx3 and Vps17 off early endosomes, we asked whether α-syn inhibits the endocytic recycling of Fet3/Ftr1. We used a Fet3-GFP strain in which the chromosomal copy of *FET3* is replaced by *FET3-GFP*. The Fet3-GFP strain behaves similar if not identical to the wild-type cells, and α-syn fails to affect the glycosylation of Fet3-GFP (Supplementary Material, Fig. S1A–D). These cells were grown in SC drop out media, which has a low concentration of iron (0.74 μM).

Western blotting was used to detect the Fet3-GFP protein in a variety of cell lysates. The Fet3-GFP protein exhibited an intense band in EV control cells (EV/−Fe), whereas the intensity of this band significantly decreased (by 36%; $P = 0.0007$) upon expression of α-syn (Fig. 5A). As a positive control, Fet3-GFP cells (EV or α-syn) incubated for 6 h in medium supplemented with 10 μM added iron exhibited almost no detectable Fet3-GFP, which is consistent with reference (45). For cells grown in minimal medium (low iron), α-syn and added iron, both independently and together, decrease the level of Fet3-GFP.

Fluorescence microscopy was also used to probe the effects of α-syn and added iron on the Fet3-GFP strain (Fig. 5B). The images in the top half of the figure were acquired after 6 h in inducing medium with 20 μM BPS (+EV/−Fe). The images in the bottom half of the figure were acquired after 6 h in inducing medium with 20 μM BPS but with the last hour in high iron (+EV/+Fe). The Fet3-GFP strain (+EV/−Fe) showed diffuse green fluorescence throughout cells as well as prominent green fluorescence around the periphery of the cells, consistent with plasma membrane localization (Fig. 5B, top panel). The mean total GFP fluorescence of each Fet3-GFP cell in various fields from three independent colonies was measured using ImageJ, and the plot of the normalized fluorescence intensity shows that α-syn caused a 61% ($P < 0.0001$) decrease in mean fluorescence (Fig. 5C) relative to control cells. Iron-shocked cells (±α-syn/+Fe) exhibited significantly less fluorescence throughout the cells compared with EV cells (compare the bottom two rows to row one). The plot in Figure 5C shows that α-syn decreases the mean Fet3-GFP fluorescence of cells to the same extent as iron. These results show that α-syn and iron shock each cause an overall decrease in Fet3-GFP fluorescence.

α-Syn mimics iron shock: both accelerate the degradation of Fet3-GFP complexes. Iron shock inhibits the endocytic recycling of Fet3/Ftr1 and shunts early endosomes containing Fet3/Ftr1 to enter the degradative pathway (45). We sought to determine whether α-syn also drives Fet3-GFP-Ftr1 complexes to the vacuole. To prevent the degradation of Fet3-GFP in the vacuole we used the Fet3-GFP *pep4Δ* strain. *PEP4* codes for the master vacuolar protease; deletion of this gene results in the failure of the vacuole to proteolyze proteins (50). It was expected that upon iron shock or α-syn expression that the Fet3-GFP protein would accumulate in the vacuole in the Fet3-GFP *pep4Δ* strain.

Figure 6 shows images of the Fet3-GFP *pep4Δ* strain (EV or α-syn) without (top panel) or with a 1 h iron-shock (bottom panel) at the end of 6 h incubation in inducing media containing 20 μM BPS. Consider the case where cells were cultured in

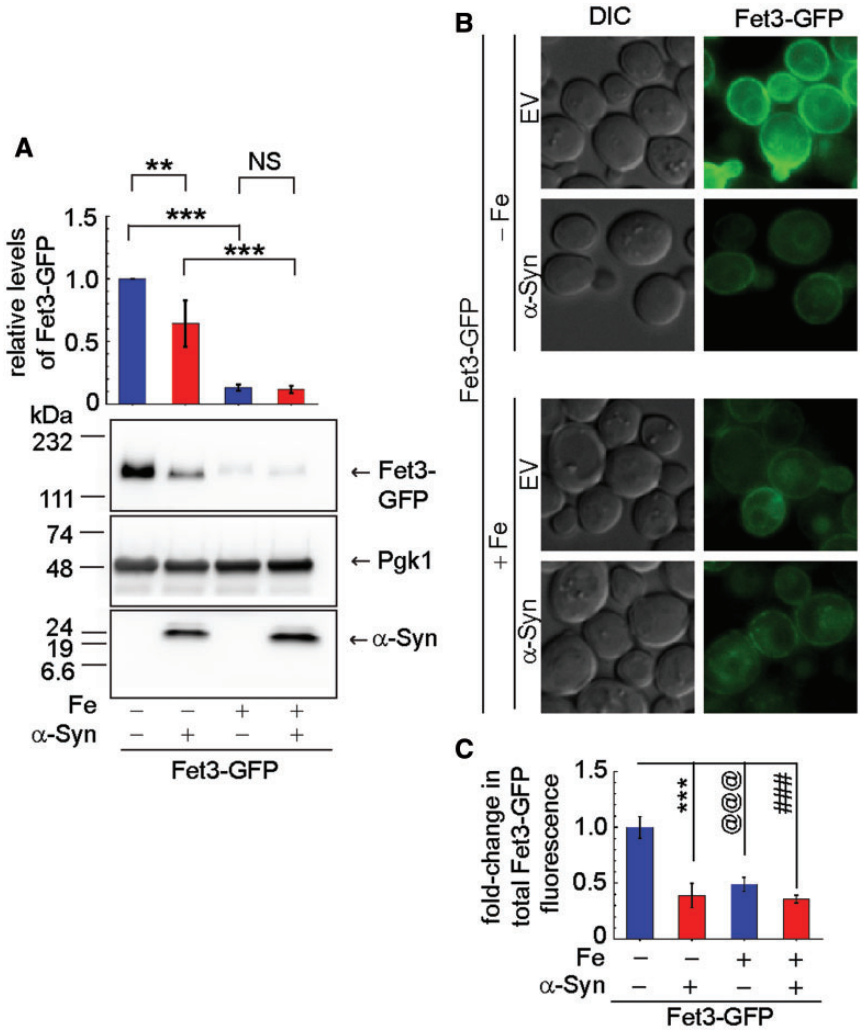

Figure 5. α-Syn mimics iron shock. (**A**) α-Syn and iron decrease the level of the Fet3-GFP protein. Cells transformed with the indicated plasmids were pre-grown in non-inducing media overnight, diluted into inducing media ± 10 μM ferric iron, and induced for 6 h. Cells were lysed, subjected to SDS-PAGE, followed by western blotting using an antibody against GFP. Pgk1 was the loading control. Plot of total Fet3-GFP levels normalized to Pgk1 is at the top of western blot panel. Values are means ± SD of three independent colonies. $^{**}P = 0.0007$; $^{***}P < 0.0001$; NS, non-significant was determined by one-way ANOVA with Bonferroni correction. (**B**) α-Syn decreases the Fet3-GFP fluorescence on the cell periphery. Top panel (–Fe): Fet3-GFP cells transformed with the indicated plasmids were pre-grown in non-inducing media overnight, diluted into inducing media containing 20 μM BPS, and induced for 6 h. Bottom panel (+Fe, iron shock): Fet3-GFP cells were treated the same as above except that during the last hour of incubation cells had an iron shock (500 μM ferric ammonium citrate). Cells were imaged by fluorescence microscopy. (**C**) Plot of normalized mean Fet3-GFP fluorescence intensity of individual cells (B). Values are mean ± SD of three independent colonies. A one-way ANOVA with a Bonferroni correction was used to determine significance. $^{***}P = 0.0004$; $^{@@@}P \leq 0.0001$; $^{###}P = 0.0009$.

inducing media with no iron shock. In EV control cells green fluorescence from Fet3-GFP proteins is prominent on the cell periphery, consistent with plasma membrane association, and in the vacuole (Fig. 6A, first row). In α-syn-expressing cells green fluorescence from the Fet3-GFP proteins localizes mainly to the vacuole with negligible fluorescence on the cell periphery (Fig. 6A, second row). For both experiments, fluorescence intensity was measured on the cell periphery and in the vacuole, and the resulting ratios of cell periphery-to-vacuolar fluorescence are shown in Figure 6B. In the absence of added iron, α-syn caused a significant decrease ($P = 0.0043$) in the ratio of cell periphery-to-vacuolar fluorescence, consistent with α-syn driving the Fet3-GFP protein from the plasma membrane to the vacuole.

In the case of iron shock, when Fet3-GFP *pep4*Δ cells (EV or α-syn) were subjected to a 1 iron shock the Fet3-GFP fluorescence disappeared from the plasma membrane and appeared in the vacuole. A plot of the cell periphery-to-vacuole fluorescence revealed a significant decrease in this ratio for the two iron-shocked samples compared with EV control cells (Fig. 6B). Western blotting showed that α-syn decreased the level of Fet3-GFP in WT cells but not in *pep4*Δ cells that have defective vacuoles (Fig. 6C), as expected. Collectively, the results show that α-syn and a high iron shock are functionally equivalent, in that, each accelerates the degradation of Fet3/Ftr1 complexes. The question is, does α-syn accelerate the degradation of Fet3/Ftr1 complexes that emanate from the plasma membrane or from complexes from the biosynthetic pathway?

α-Syn accelerates the degradation of Fet3/Ftr1 complexes that emanate from the plasma membrane. Our data have revealed that Fet3/Ftr1 is more rapidly degraded in cells expressing α-syn than in control cells. The issue is whether the complexes affected by α-syn emanate from the plasma membrane, i.e. the endocytic recycling pathway or from the biosynthetic pathway.

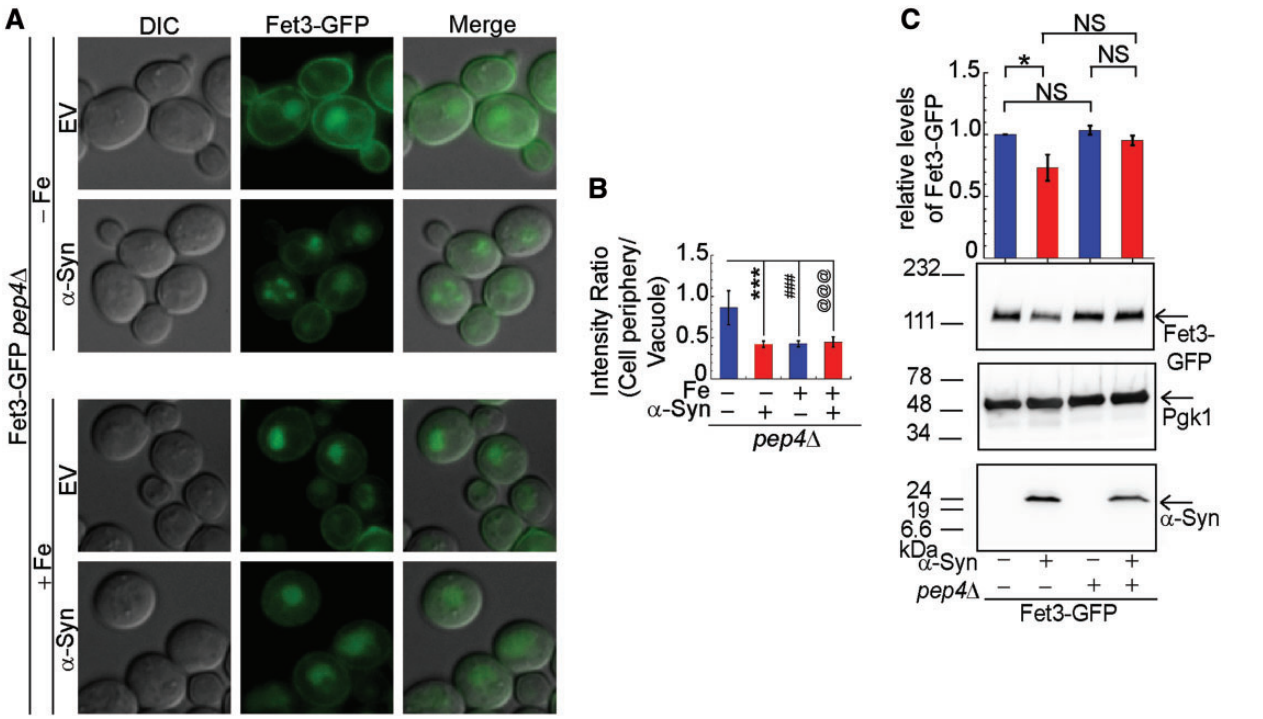

Figure 6. α-Syn targets Fet3-GFP to the vacuole. (**A**) α-Syn targets Fet3-GFP to the vacuole. Fet3-GFP *pep4*Δ cells transformed with the indicated plasmids were cultured as described in Figure 5B, and then imaged using fluorescence microscopy. (**B**) Plot of mean Fet3-GFP fluorescence on the cell periphery to mean Fet3-GFP fluorescence in the vacuole from panel (A). Values are means ± SD of three independent colonies, Significance was determined by a one-way ANOVA with Bonferroni correction. $^{***}P = 0.0043$; $^{\#\#\#}P = 0.0039$; $^{@@@}P = 0.0057$. (**C**) Western blot of lysates from wild-type and *pep4*Δ cells ± α-syn. Cells with the indicated plasmids were pre-grown overnight in non-inducing media, diluted into inducing media with 20 μM BPS and grown for 6 h at 30°C. Pgk1 is the loading control. Plot shows normalized levels of Fet3-GFP (Fet3-GFP/Pgk1; determined by ImageJ). Values are means of three independent colonies. A one-way ANOVA with Bonferroni correction was used to determine significance: $^{*}P = 0.0121$. NS, not significant.

In this latter case, perhaps α-syn blocks the transport of newly synthesized Fet3-GFP-Ftr1 complexes to the plasma membrane and instead redirects them to the vacuole. This issue was addressed in two ways.

First, fluorescence microscopy was used to monitor the Fet3-GFP signal on the cell plasma membrane in cells with or without α-syn expression after treatment of the cells with cycloheximide. A complication of such an experiment is that there is no appreciable Fet3-GFP fluorescence on the cell periphery to monitor when α-syn expressing cells are incubated for 6 h in SC-2% Gal (+chelator) media (see Fig. 6A α-syn/−Fe). We reasoned that if the expression of α-syn could be lowered in the cells, then after 6 h incubation cells should display more Fet3-GFP fluorescence on the plasma membrane. To lower α-syn expression, the cells were thus incubated in SC-1% (rather than 2%) Gal media with chelator, and this strategy yielded significantly more Fet3-GFP fluorescence on the plasma membrane.

Figure 7A shows changes in fluorescence of Fet3-GFP *pep4*Δ cells ± α-syn after the addition of cycloheximide. The membrane fluorescence decay curves are shown in Figure 7B. With the biosynthetic pathway shut down, the decay curves represent at minimum three processes (Fig. 1B): first, endocytosis (removal of cargo from the plasma membrane), second, recycling (return of the cargo to the plasma membrane) and third, transit of the cargo to the vacuole. The endocytosis of Fet3-GFP/Ftr1 complexes decreases the Fet3-GFP fluorescence on the plasma membrane, whereas the recycling of the complexes restores the fluorescence on the plasma membrane. Over time, a decay in fluorescence occurs because a fraction of the internalized complexes are sorted to the vacuole in EV control cells; hence, the rate of loss of Fet3-GFP fluorescence on the plasma membrane (owing to endocytosis) is greater than the rate of gain of Fet3-GFP fluorescence on the plasma membrane (owing to recycling). We hypothesize that a significantly larger fraction of the internalized complexes are sorted to the vacuole in α-syn-expressing cells because α-syn blocks the binding of Snx3 and Vps17 to early endosomes (Fig 2). Notably, at 2 and 4 h the fluorescence intensities of the α-syn decay curve are significantly lower in magnitude compared with same points on the control curve (Fig. 7B). This finding is consistent with α-syn accelerating transit to the vacuole of complexes that emanate from the plasma membrane. The Fet3-GFP protein level was unaffected because *PEP4* was deleted (Fig. 7C), and α-syn levels after the treatment with cycloheximide are shown in Figure 7C.

Second, the TSY145 strain was used to probe the role of ubiquitylation of Fet3 and Ftr1 on endocytosis, recycling and entry into the MVB pathway (27). In this strain, the lysineless Fet3/Ftr1 proteins are fully functional (Supplementary Material, Fig. S1C) and they are constitutively recycled by the Snx3–retromer pathway even in the presence of high iron. Thus, the lysineless mutants are endocytosed independent of ubiquitylation; however, the cytosolic lysine residues are required—most likely because they are ubiquitylated—for targeting Fet3/Ftr1 complexes into the MVB pathway (27).

If α-syn functions in a similar manner to iron shock, then expressing α-syn in the TSY145 strain should fail to drive the lysineless Fet3/Ftr1 complexes into the MVB degradative pathway. Indeed, α-syn failed to alter both the plasma membrane

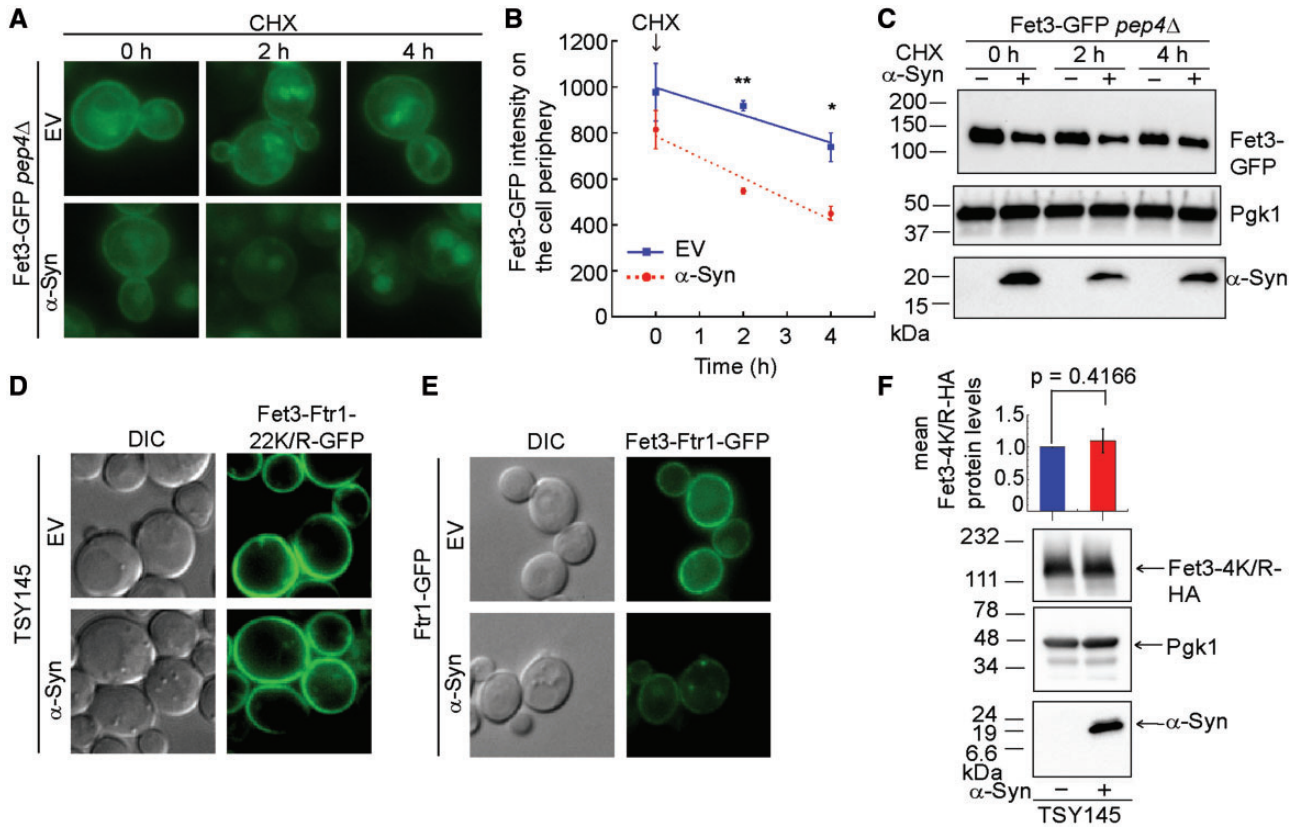

Figure 7. α-Syn accelerates the degradation of Fet3/Ftr1 complexes that emanate from the plasma membrane. (**A**) α-Syn decreases the Fet3-GFP intensity on the plasma membrane post-cycloheximide (CHX) treatment. Fet3-GFP *pep4*Δ cells were transformed with indicated plasmids and cultured in inducing media with 1% galactose for 6 h. At 6 h, CHX (100 μg/ml) was added, and cells were imaged by fluorescence microscopy at the indicated time points. (**B**) Plot of mean Fet3-GFP fluorescence on the cell periphery from panel (A). Values are means ± SD of three independent experiments. A Student's *t*-test was used to determine *P* values: $^{**}P = 1.4 \times 10^{-5}$; $^{*}P = 0.0019$. (**C**) Western blot of lysates from panel (A). Lysates were subjected to SDS-PAGE followed by western blotting. Pgk1 is the loading control. The images are representative of two independent experiments. (**D**) Ubiquitylation of Fet3/Ftr1 after endocytosis is required for α-syn to drive the iron importers into the MVB pathway. Fluorescence microscopy of TSY145 strain, which contains Fet3(4K/R)-3HA and Ftr1(18K/R)-GFP, with or without α-syn after 5 h in the inducing media with 20 μM BPS shows that α-syn had no effect on the Fet3/Ftr1–22K/R-GFP fluorescence. (**E**) Fluorescence microscopy of Fet3/Ftr1– GFP strain (±α-syn) after 5 h in the inducing media with 20 μM BPS shows that α-syn abolishes the Ftr1– GFP fluorescence. (**F**) Western blot of TSY145 cell lysate. Cells were cultured as in (D). Pgk1 was the loading control. Plot of normalized Fet3–4K/R-HA protein level is on the top of western blot. Values are means ± SD of three independent colonies. *P* value determined using a Student's *t*-test.

localization of the fluorescently tagged lysineless Fet3/Ftr1 complexes and the protein level of lysineless Fet3 (Fig. 7D–F). As a control, α-syn dramatically altered the plasma membrane localization and overall fluorescence intensity of wild-type Fet3/Ftr1-GFP (Fig. 7E), which is similar to what we found for the effect of α-syn on Fet3-GFP (Figs 5 and 6).

Knocking down the sorting nexin snx-3 disrupts iron homeostasis in a Caenorhabditis elegans model of neurodegeneration. To extend the findings from yeast, we turned to a *C. elegans* PD model that enables dopaminergic neurodegeneration to be monitored. The evolutionarily conserved retromer complex associates with cargo adaptors like sorting nexins, which regulate retrograde endosome-to-trans-Golgi transport of different protein cargoes (41). Although, there is lack of knowledge regarding retromer-mediated retrograde transport of iron transporters in *C. elegans*, the Snx3–retromer complex plays an important role in maintaining iron homeostasis by regulating the endocytic-recycling of iron transporters in mammalian cells. Studies suggest that Snx3–retromer complex retrieves transferrin receptor (TfR) (51) and the divalent metal ion transporter 1 (DMT1) (52,53) from endocytic vesicles and prevents their lysosomal degradation. The transferrin–TfR system is a major route of iron uptake in mammalian cells. Iron efflux from endosomes containing iron and transferrin–TfR complexes into the cytoplasm is mediated by DMT1. Many studies have focused on understanding the trafficking of DMT1 because high levels of DMT1 have been associated with iron neurotoxicity and neurodegeneration in different PD models (54,55). DMT1 is a canonical substrate of Snx3 and has also been studied extensively to understand the structural dynamics of Snx3–retromer complex (56,57). A recent study has found that α-syn facilitates iron uptake through TfR and modulates retinal iron homeostasis (58). Another study suggests that TfR deficiency causes iron deficiency and neurodegeneration in mice (59). The amyloid precursor protein (APP) stabilizes the iron exporter ferroportin on the plasma membrane (60), and retromer facilitates iron export through ferroportin by regulating the recycling of APP (34,61,62). There is a growing consensus of the importance of APP in maintaining iron homeostasis because the loss of APP has been associated with defects in ferroportin-mediated iron export (63–65). Apart from APP, the iron export through ferroportin is mediated by the ferroxidase activity of ceruloplasmin and loss of functional ceruloplasmin is associated with the cellular iron retention and PD (66–71). Although, a recent study suggests that loss of TfR and not ferroportin causes neurodegeneration in mice (59). Overall, these studies show that disturbances in the function/

Table 2. Iron transporters investigated in this study

Protein	Function	Orthologs
Ftr1 (yeast)	Ftr1 is membrane-bound iron permease that mediates iron import by working in concert with Fet3. Ftr1 binds to Snx3 sorting nexin and gets recycled back to plasma membrane with Fet3.	No ortholog of Ftr1 in worms or humans
Fet3 (yeast)	Fet3 is a membrane-bound, multi-copper oxidase (MCO)that mediates iron import by working in concert with Ftr1.	The worm ortholog of Fet3 is F21D5.3. (A BLAST search query of Fet3 sequence against the *C. elegans* protein database yielded F21D5.3 [Score: 96.7; E value: 1e-20]). The human orthologs of Fet3 are ceruloplasmin and hephaestin.
SMF-3 (worms)	This is the presumed iron importer in worms.	The human ortholog of SMF-3 is DMT1 DMT1 proteins either export divalent metals out of endosomes or they embed in the plasma membrane and import iron into cells DMT1 isoform II is the human divalent metal ion transporter. DMT1-II is a substrate of human Snx3.
Fpn1.1 (worms)	Ferroportin is the only known iron exporter in eukaryotes. It works in concert with a MCO to mediate iron export. Ferrous ions transit through ferroportin molecules and are subsequently oxidized by the MCO to ferric ions.	No orthologs in yeast. The human ortholog of Fpn1.1 is ferroportin (FPN).
F21D5.3 (worms)	We hypothesize that F21D5.3 (MCO) and Fpn1.1 form a membrane-bound complex and mediate iron export in worm dopaminergic neurons	The human orthologs of F21D5.3 is ceruloplasmin and hephaestin. The putative worm F21D5.3/Fpn1.1 complex would be analogous to the human hephaestin/ferroportin complex that mediates iron export.

trafficking of iron transporters play a role in inducing iron neurotoxicity and neurodegeneration. On the basis of our results from yeast, we reasoned that because iron transporters are substrates for Snx3–retromer complex, and retromer complex is evolutionarily conserved, α-syn likely disrupts iron homeostasis in a complex eukaryotic animal like *C. elegans* by inhibiting the SNX-3-retromer mediated retrograde transport of iron transporters. Table 2 presents the list of iron transporters investigated in this study. We reasoned that if iron transporters are substrates of SNX-3, then the depletion of *snx-3* gene product activity should cause the iron transporter to be degraded in the lysosome. The effect of cell-specific knock down of *snx-3* in worm DA neurons with or without the expression of α-syn was evaluated. If SNX-3 facilitates the recycling of *iron importers*, then knocking down *snx-3* should cause iron importers to be degraded in the lysosome; such neurons might become iron deficient, and an iron chelator would exacerbate neurodegeneration. Conversely, if SNX-3 facilitates the recycling of *iron exporters*, then knocking down *snx-3* might cause the iron exporters to be degraded in the lysosome; such neurons would accumulate iron, and, in this case, an iron chelator would rescue neurodegeneration. The iron chelator desferoximine (DFO) facilitates assessment of iron homeostasis, with the extent of dopaminergic neurodegeneration serving as a surrogate marker of iron homeostasis.

We asked whether the depletion of *snx-3* using RNAi knockdown enhances the degeneration of dopaminergic neurons in the absence of α-syn. Strain UA202 (*sid-1(pk3321)*; *vtIs7*[P*dat-1*:: GFP]; *baIn36*[P*dat-1*:: *sid-1*, P*myo-2*:: mCherry]) (72,73) was used for this purpose. These worms were designed to uptake dsRNA exclusively in the DA neurons (74). Conditional RNAi knockdown of *snx-3* did not alter dopaminergic neurodegeneration at day 7 of development compared with the same worms treated with RNAi bacteria that do not express any dsRNA clone (EV) (Fig. 8A). In contrast, knockdown of *mcu-1*, a mitochondrial calcium uniporter and positive control for neurodegeneration, caused significant dopaminergic neuron loss at day 7.

In parallel, a dopaminergic RNAi-specific strain that expresses both GFP and α-syn in the DA neurons (UA196 (*sid-1(pk3321)*; *baIn11*[P*dat-1*::α-syn, P*dat-1*:: GFP]; *baIn33*[P*dat-1*:: *sid-1*, P*myo-2*:: mCherry]) was used to examine if the knockdown of *snx-3* exacerbates α-syn neurotoxicity. This strain also selectively uptakes RNAi in DA neurons. We found that 34% of the α-syn-expressing animals displayed normal neurons, and this percentage decreased to 16%, when the same animals were treated with *snx-3* dsRNA ($P < 0.05$; one-way ANOVA) (Fig. 8B). DFO rescued DA neurons expressing α-syn compared with the EV controls (Fig. 8C). DFO also rescued against neurodegeneration in α-syn expressing worms with *snx-3* knocked down (22–44%), and the amount of rescue was similar to the EV controls, where 50% of this population exhibited normal neurons following the DFO treatment (Fig. 8C). Representative images of worms with the various treatments described earlier are shown in Figure 8D. These results are consistent with the α-syn-expressing worms reproducibly displaying progressive loss of dopaminergic neurons as they age, as previously reported (75,76). Moreover, the dopaminergic neurons appear to accumulate iron, as judged by the rescue by DFO, and *snx-3* depletion accelerates dopaminergic neuron cell loss, whereas chelator conversely rescues DA neuron loss with or without *snx-3* depletion.

Knocking down the iron importer SMF-3 *rescues α-syn-induced neurodegeneration*. The findings that DFO rescues neurodegeneration in α-syn expressing dopaminergic neurons (EV/*snx-3* RNAi) raises the possibility that iron accumulates in these

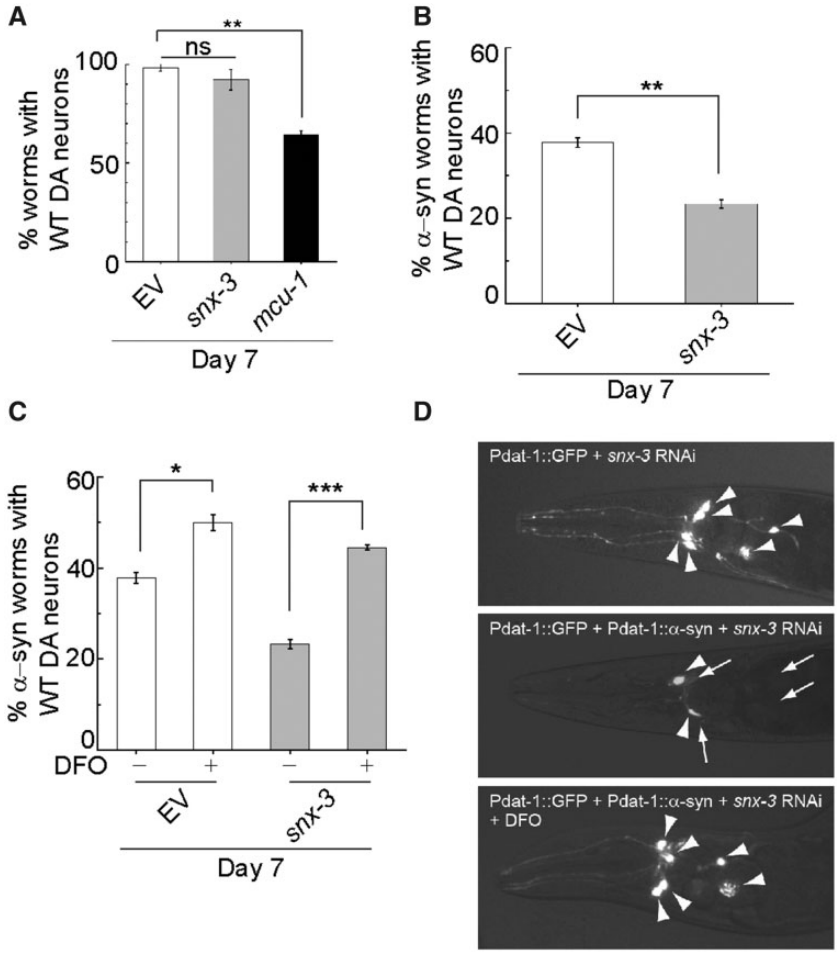

Figure 8. Depletion of *snx-3* in *C. elegans* dopaminergic neurons enhances neurodegeneration in α-syn-expressing worms. (**A**) GFP-expressing worms (strain UA202) with *snx-3* depleted showed no neurodegeneration, similar to EV control cells in 7-day-old worms. As a positive control, depletion of *mcu-1* caused significant loss of the GFP-only DA neurons. RNAi bacteria which does not express any clone is denoted 'EV' for empty vector. Data are mean ± SD ($N = 3$), 30 worms in triplicate. $^{ns}P > 0.05$, $^{**}P < 0.01$, as determined by one-way ANOVA, Sidak's multiple comparisons test. (**B**) Plot shows the percentage of 7-day old worms with WT dopaminergic neurons expressing α-syn (strain UA196) following RNAi targeting *snx-3*. Data are mean ± SD ($N = 3$), 30 worms in triplicate. $^{**}P < 0.01$, as determined by one-way ANOVA, Sidak's multiple comparisons test. (**C**) DFO partially rescues neurodegeneration because of the depletion of *snx-3* in *C. elegans* dopaminergic neurons expressing α-syn. Plot shows percentage of 7-day old α-syn worms with normal neurons following RNAi targeting *snx-3* with or without DFO treatment. Data are mean ± SD ($N = 3$), 30 worms in triplicate. $^{*}P < 0.05$, $^{***}P < 0.001$ and was determined by two-way ANOVA, Sidak's multiple comparisons test. (**D**) Representative images of dopaminergic neurons. Arrowheads show intact dopaminergic neuron cell bodies. Arrows indicate areas where dopaminergic neurons have degenerated. Top panel: GFP-only animal with *snx-3* silenced by RNAi in a GFP-only animal. Middle panel: Enhanced neurodegeneration in dopaminergic neurons expressing α-syn occurs following *snx-3* RNAi. Bottom panel: The chelator DFO rescues neurodegeneration of dopaminergic neurons expressing α-syn with *snx-3* RNAi.

neurons, and this may have functional consequences for α-syn-induced neurodegeneration (Fig. 8C). We reasoned that if worm dopaminergic neurons expressing α-syn accumulate iron, then knocking down the iron importer *smf-3* should rescue neurodegeneration. This idea was tested as follows.

In dopaminergic RNAi-sensitive GFP-only expressing worms (UA202), the depletion of *smf-3* had no effect on dopaminergic viability (Fig. 9A). In α-syn expressing worms (strain UA196), at day 7 of development, only 37% of α-syn-expressing worms exhibited normal dopaminergic neurons. Notably, the depletion of *smf-3* in these animals resulted in a significant rescue of dopaminergic neurodegeneration, where 54% of α-syn-expressing worms had normal dopaminergic neurons (Fig. 9B). RNAi targeting of *cua-1*, encoding a copper transporter, did not result in a similar response. Thus, the selective rescue observed by knocking down *smf-3* implies that worm dopaminergic neurons expressing α-syn accumulate iron and that iron enhances α-syn-induced neurotoxicity.

Given that knocking down the iron importer rescues α-syn-induced neurodegeneration, we sought to determine whether RNAi depletion of the iron exporter ferroportin *fpn1.1* and the putative ferroxidase F21D5.3 would exacerbate dopaminergic neurodegeneration.

Knocking down iron exporters (F21D5.3 or fpn1.1) exacerbates α-syn-induced neurodegeneration; the iron chelator DFO rescues. We first determined that RNAi depletion of F21D5.3 or *fpn1.1* in GFP-only expressing worms (UA202) failed to cause dopaminergic neurodegeneration compared with EV controls (Fig. 9A).

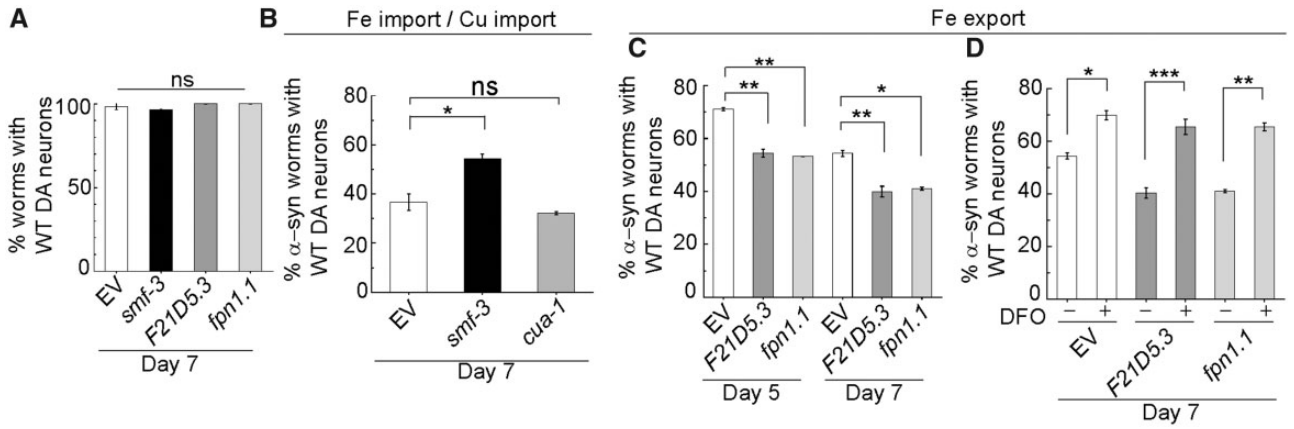

Figure 9. Interactions between α-syn and iron import and iron export genes. (**A**) Depletion of *smf-3* (DMT1), F21D5.3 (*FET3/Cp*) or *fpn1.1* in *C. elegans* dopaminergic neurons fails to induce neurodegeneration in the absence of α-syn. The plot shows percentage of the worm population exhibiting a full complement of dopaminergic neurons in 7-day-old worms following RNAi targeting of these genes in UA202 worms that express GFP only. A worm was scored as normal if it retained the full complement of six dopaminergic neurons (WT dopaminergic neurons). Plot shows percentage of 7-day-old worms with normal neurons. Data are mean ± SD ($N = 3$), 30 worms in triplicate. $^{ns}P > 0.05$ determined by one-way ANOVA, Sidak's multiple comparisons test. (**B**) Depletion of *smf-3* partially rescues neurodegeneration in *C. elegans* dopaminergic neurons expressing α-syn. Plot shows percentage of 7-day-old α-syn worms (strain UA196) with normal neurons following RNAi targeting *smf-3*. RNAi knockdown of *cua-1*, a negative control, did not impact neurodegeneration in α-syn worms. Data are mean ± SD ($N = 3$), 30 worms in triplicate. $^{*}P < 0.002$ determined by a Student's *t*-test. (**C**) Depletion of F21D5.3 or *fpn1.1* in *C. elegans* dopaminergic neurons enhances neurodegeneration in the presence of α-syn. Plot shows the percentage of 5- and 7-day-old worms with WT dopaminergic neurons expressing α-syn (strain UA196) following RNAi targeting F21D5.3 or *fpn1.1*. Data are mean ± SD ($N = 3$), 30 worms in triplicate. $^{*}P = 0.013$; $^{**}P < 0.003$ and was determined by one-way ANOVA, Tukey's multiple comparisons test. (**D**) DFO partially rescues dopaminergic neurodegeneration induced by depletion of F21D5.3 or *fpn1.1* in *C. elegans* expressing α-syn. Plot shows percentage of 7-day-old α-syn worms with normal neurons following RNAi targeting F21D5.3 or *fpn1.1* with or without DFO treatment. Data are mean ± SD ($N = 3$), 30 worms in triplicate. $^{*}P < 0.05$; $^{**}P < 0.01$; $^{***}P < 0.001$ and was determined by two-way ANOVA, Sidak's multiple comparisons test.

We next analyzed neurodegeneration in α-syn-expressing worms (UA196) with or without RNAi depletion of F21D5.3 or *fpn1.1*. At day 5, 71% of the α-syn/EV worms exhibited a full complement of intact dopaminergic neurons, whereas 54% of both the α-syn/F21D5.3 RNAi and α-syn/*fpn1.1* RNAi worms displayed a full complement of dopaminergic neurons (Fig. 9C; EV RNAi). At day 7, 40% and 41% of F21D5.3 and *fpn1.1* depleted populations, respectively, displayed a normal complement of neurons, compared with 54% in the EV control α-syn-expressing worms (Fig. 9C).

Knocking down iron exporters in DA neurons should cause iron to accumulate, which should accelerate cell loss. To test this hypothesis, transgenic worms expressing α-syn in dopaminergic neurons were divided into three treatment groups: EV, F21D5.3 dsRNA, and *fpn1.1* dsRNA. Each group was treated with the solvent vehicle (water) or 100 μM DFO, and worms were evaluated at day 7. For the α-syn/EV group, 54% of the population displayed normal neurons, and treatment of this group with DFO increased the population of worms with intact neurons to 71%. For the two knockdown groups, α-syn/F21D5.3 RNAi and α-syn/*fpn1.1* RNAi, 40% and 41% of the populations, respectively, retained a full complement of neurons (Fig. 9D) ($P < 0.05$, one-way ANOVA), and DFO significantly increased the percentage of worms displaying a full complement of DA neurons in both groups to approximately 70%. These results show exacerbated neurotoxicity of α-syn upon depletion of iron exporters.

Discussion

We have discovered that α-syn inhibits Snx3–retromer-mediated endocytic recycling of Fet3/Ftr1 complexes in yeast. Moreover, α-syn phenocopies iron shock in this model, as it inhibits the retromer-mediated retrieval of Fet3/Ftr1 from the degradative pathway (Figs 1, 2 and 5–7). At a molecular level, this is the first report to show that α-syn drives Snx3 and Vps17 off endocytic vesicles, most likely by blocking the binding of Snx3 to PI3P-containing endosomes (Figs 2–4). We propose that blocking the binding of Snx3 and Vps17 to early endosomes prevents retromer from retrieving Fet3/Ftr1 from the degradative pathway. This represents a putative molecular mechanism underlying neurotoxicity whereby mediators of iron homeostasis intersect with genetic (α-syn) modulators of PD.

α-Syn alters the endocytic recycling of Fet3/Ftr1 complexes. We have shown that α-syn accelerates the degradation of Fet3/Ftr1 complexes in yeast cells (Fig. 7A–C). We hypothesized that the accelerated degradation is due to α-syn interfering with the retromer-mediated endocytic recycling pathway (see Introduction and Fig. 1B), but the possibility that α-syn interferes with the biosynthetic pathway was also considered. The biosynthetic pathway transits newly synthesized proteins to different destinations in the cell. In the case of Fet3/Ftr1, the newly synthesized complexes transit through the secretory pathway to the plasma membrane. Perhaps α-syn, a non-native protein expressed in yeast, disrupts the biosynthetic pathway such that a fraction of the Fet3/Ftr1 complexes inside the cell fail to reach the plasma membrane; the complexes instead divert to the vacuole for degradation. This possibility was ruled out for the following reasons. (i) Cycloheximide was employed to shut down the biosynthetic pathway. With the biosynthetic pathway shut down, α-syn significantly accelerated the degradation of complexes that emanated from the plasma membrane compared with EV control cells (Fig. 7A–C). These results demonstrate that α-syn interferes with recycling. (ii) Iron shock has been shown to inhibit the endocytic recycling of Fet3/Ftr1, which causes the complexes to transit to the vacuole for

degradation (26). We showed that α-syn and a high iron shock have almost identical effects on Fet3-GFP localization and protein levels (Figs 5, 6 and 7D–F). Such close mimicry suggests that α-syn and high iron alter the same pathway, i.e. recycling. (iii) Snx3–retromer mediates the endocytic recycling of Fet3/Ftr1 complexes (26,27). Snx3 binds to early endosomes via its PX domain, which selectively binds PI3P, and Snx3 binds to an endocytic recycling sequence on Ftr1 (26). This is the first report to show that α-syn blocks the binding of Snx3 to vesicles *in vivo* and *in vitro*. By blocking the interaction of Snx3 (and Vps17) with early endosomes, we propose that the retromer machinery fails to retrieve Fet3/Ftr1 complexes from the degradation pathway. These results are consistent with α-syn interfering with recycling. (iv) Fet3 is a glycoprotein. Fet3 must be glycosylated in order to efficiently traffic (with Ftr1) through the secretory pathway to the plasma membrane (77). We asked whether α-syn inhibited the glycosylation of Fet3 but found no evidence of altered glycosylation of Fet3-GFP in cells expressing α-syn (Supplementary Material, Fig. S1D). Overall, the data in Figures 2–7 are consistent with α-syn interfering with retromer-mediated endocytic recycling of Fet3/Ftr1. After the endocytosis of Fet3/Ftr1 complexes in cells that express α-syn, we propose that two events must occur for the complexes to transit to the vacuole: α-syn must block the binding of Snx3/Vps17 to early endosomes, and subsequently the Fet3/Ftr1 proteins must be ubiquitylated.

Using a *C. elegans* PD model, we found that transgenic worms expressing α-syn exhibit an age-dependent degeneration of dopaminergic neurons that can be modulated by protein effectors of iron transport (Figs 8 and 9), and that some of the degeneration is rescued by the iron chelator DFO (Figs 8C and 9D). Rescue of degeneration by DFO in α-syn/EV-expressing dopaminergic neurons implies, but does not prove, that iron accumulates in these neurons with age. Our results are consistent with iron accumulation enhancing α-syn-induced neurodegeneration (Figs 8C and 9D), and that α-syn is responsible for the iron accumulation because there is no appreciable degeneration of dopaminergic neurons in control worms without α-syn (Figs 8A and 9A). These results are consistent with α-syn causing dysregulated iron homeostasis in dopaminergic neurons, which over time, leads to the accumulation of iron and enhanced cytotoxicity of α-syn.

The simplest interpretation of the *C. elegans* results are that α-syn perturbs SNX-3 retromer endocytic recycling of ferroportin, FPN1.1, and/or the ceruloplasmin-like ferroxidase F21D5.3, and that this perturbation drives one or both proteins to the lysosome for degradation. Dopaminergic neurons expressing α-syn would therefore have a deficit of the exporter and/or its ferroxidase, and such neurons would exhibit iron neurotoxicity, which would exacerbate α-syn cytotoxicity. An iron chelator would be predicted to rescue this effect, which it did (Figs 8 and 9). In short, the same mechanism operates in yeast and worms, except that α-syn inhibits Snx3/SNX-3-mediated endocytic recycling of iron *importers* in yeast and iron *exporters* in worms.

Two limitations of the experiments with *C. elegans* relate to the small number of cells that we probed. Only 8 of ∼1000 worm cells are dopaminergic neurons. One limitation is that we could not determine whether α-syn and the various knockdowns change the iron content of the individual dopaminergic neurons. As such, our findings that DFO and *smf-3* RNAi partially protect against α-syn-induced neurodegeneration imply, but do not prove, that such neurons accumulate iron. The other limitation is that we could not determine whether α-syn decreases the protein levels of FPN1.1, F21D5.3 or SMF-3 in this small number of neurons. Because we cannot make any statement about changes in the levels of these three proteins, we cannot rule out that α-syn increases iron import (rather than decreasing iron export) in worm dopaminergic neurons. For example, *DMT1*, which is the human ortholog of *smf-3*, has been found to increase in the brain with age (78). In mice, mutations in parkin, which is a gene associated with early-onset PD, cause proteasome inhibition and an increased level of DMT1 (79). Given that α-syn inhibits the proteasome (80), perhaps α-syn inhibits the proteasome in dopaminergic neurons and this increases the level of SMF-3 (DMT1), thus enhancing iron import and causing iron neurotoxicity. Thus, knockdown of *smf-3* should rescue degeneration of dopaminergic neurons expressing α-syn in this scenario, which it did (Fig. 9B). Additional experiments in worms or mammalian cells are needed to distinguish between these two models.

It is useful to compare our results on α-syn and Snx3–retromer recycling of Fet3/Ftr1 to that of Snx3–retromer recycling of membrane proteins in human cells. First, as mentioned previously, PD-linked mutations occur in the conserved gene *VPS35* (28–30), which encodes a cargo-recognition component of retromer. The Vps35 R524W variant causes late-onset, autosomal dominant PD. The expression of Vps35 R524W in HeLa cells disrupts the recruitment of retromer to the endosomal membrane and causes the mistrafficking of the cation-independent mannose-6-phosphate receptor and the lysosomal protease cathepsin D (81), resulting in the formation of α-syn aggregates. (In worms, cathepsin D RNAi also leads to α-syn accumulation (82).) Second, in the Wnt signaling pathway, the Wntless receptor (Wls) undergoes retromer-mediated recycling between the Golgi and the plasma membrane. Wls is a canonical substrate of human Snx3 (41,83). A recent study showed that knocking down Snx3 by siRNA results in the mistrafficking of Wls to the lysosome (83). Third, a shRNA-based screen in human H4 neuroglial cells identified endocytic recycling pathway components as genetic modifiers of α-syn aggregation, secretion and toxicity (32). Our interpretation of these results is that retromer-mediated recycling of receptors/transporters can be disrupted by knocking down a component of retromer, by mutating a component or retromer, and even by α-syn interfering with the binding of the retromer component Snx3 to early endosomes (Fig. 10). In sum, our results raise the possibility that by inhibiting Snx3–retromer-mediated endocytic recycling of iron transporters, α-syn can dysregulate iron homeostasis, with functional implications for neurodegeneration.

Materials and Methods

Yeast strains, media and antibodies. Table 1 lists the strains and plasmids used in this study. All reagents unless otherwise noted were purchased form Sigma Aldrich. Liquid and solid nutrient rich complete medium (YPD) and synthetic complete (SC) drop out medium were prepared as described (84). Two plasmids were used. pAG426, which has a *URA3* selectable marker, is the EV plasmid, and pAG426-α-syn harbors the gene for human wild-type α-syn, whose expression is controlled by the *GAL1* promoter. Cells were transformed with plasmids using lithium acetate method (84). Unless stated otherwise, for all experiments, the transformants were pre-grown in non-inducing media, i.e. SC-Sucrose (SC-Suc) liquid drop out (-uracil) medium until mid-log phase to maintain the selection of plasmids and then centrifuged. α-Syn expression was induced by replacing sucrose with galactose (2%, wt/vol) (SC-Gal, inducing media)

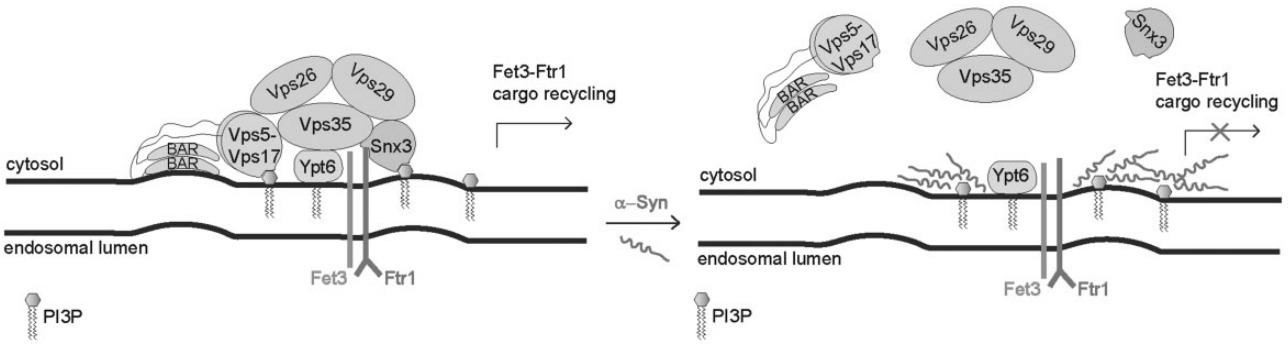

Figure 10. Model for α-syn disrupting Snx3–retromer-mediated recycling of membrane proteins. Left panel: Snx3–retromer complex binds to the C-terminus of Ftr1, which results in the formation of tubular endosomes from which vesicles containing the Fet3/Ftr1 cargo bud off and transit to the trans-Golgi. From the trans-Golgi, Fet3/Ftr1 laden vesicles transit back to the plasma membrane. Right panel: α-syn inhibits the binding of Snx3 and Vps17 to vesicles containing PI3P. Lack of Snx3 and Vps17 binding to the surface of early endosomes results in the inability of retromer to retrieve Fet3/Ftr1 from the degradative pathway.

(84). For inducing iron deficiency, the iron Fe^{+2} chelator-bathophenanthroline disulfonic acid trihydrate (BPS) was added to SC-Gal medium to a final concentration of 20 μM along with 1 mM sodium ascorbate (27). For supplementing iron, ferric chloride or ferric ammonium citrate (MP Biomedicals, #0215804090) was added to the SC-Gal medium. All experiments were conducted using single yeast colonies.

The primary antibodies used were mouse anti-α-Syn (SantaCruz, # SC-12767, BD Biosciences, # 610786), mouse anti-GFP (SantaCruz; Cat. No. SC-9996), mouse anti-Pgk1 (Abcam, # ab113687), mouse anti-mCherry (Chromotek, 6g6–20). The secondary antibody was goat anti-mouse (Santa Cruz, # SC-2005).

Western blotting. Preparation of yeast cell lysates, SDS/PAGE, and Western blot analysis was carried out as described previously (85) with only minor modifications. The western blot images were acquired using Biorad Chemidoc-MP imaging system and the intensities of Fet3-GFP and Snx3-mCherry and Vps17-mCherry were quantified by densitometry using Image J software as described (86). In our semi-quantitative analysis of band intensities in western blots, we normalized band intensities of proteins of interest to the intensity of the housekeeping protein Pgk1. We verified that Pgk1 intensity is not subject to significant variation for the conditions used herein. The normalized levels of Fet3-GFP, Snx3-mCherry or Vps17-mCherry were determined by the equation $(I_{Fet3\text{-}GFP}/I_{Pgk1})$α-syn/$(I_{Fet3\text{-}GFP}/I_{Pgk1})$ EV, where I is band intensity. For probing Fet3-GFP during iron supplementation, cells were inoculated in SC-Gal medium with or without 10 μM $FeCl_3$, respectively. For iron shock, cells were washed once with water and then incubated in SC media containing 500 μM ferric ammonium citrate with 1 mM sodium ascorbate for 1 h. For probing Snx3-mCherry, the TSY145 strain was grown overnight in SC-glucose followed by diluting it in fresh SC-Glu for 6 h and then shifting it to SC-Gal for 4 h at 30°C. Before inoculating/shifting cells, the SC-Glu/SC-Gal medium was made iron deficient by adding 20 μM BPS and 1 mM sodium ascorbate.

Fluorescence microscopy. Fluorescence images of yeast cells were acquired using an Olympus AX70 microscope equipped with an Olympus UPlanFl 100×/1.35 NA objective and a CoolSNAP HQ CCD camera (Roper Scientific). A 89021-filter set (Chroma technology) was used for GFP and mCherry detection. Images were acquired at room temperature. Images were binned (2 × 2) and acquired by 3D capture mode spanned across nine planes along the z-axis, with the inter-planar distance of 0.5 μm. Slidebook, version 4.0 (Intelligent Imaging Innovations) software was used to control image acquisition and the z-axis stepping motor (LudI electronic products). Images were analyzed and quantified by ImageJ software (1.42v). For quantifying Fet3-GFP intensities on the cell periphery, a sub-stack (usually plane no. 4) from nine planes was selected and normalized to a constant low and high value for GFP intensities. For the Fet3-GFP strain, the total fluorescence was determined. At least 100 cells were counted per independent clone. The average intensities were then subtracted from the background intensities and corrected intensities were plotted in the form of bar graph. For quantifying Snx3-mCherry or Vps17-mCherry positive puncta, at least 100 cells per clone were counted from a single substack out of all planes after normalizing the low and high value for mCherry intensities and eliminating the background intensities. For quantifying the Snx3-mCherry puncta intensities, the entire region of puncta(s) were considered and an average value of Snx3-mCherry intensities/cell was determined and plotted in the form of bar graph.

Snx3 expression. BL21 (DE3) *Escherichia coli* cells (Novagen) were transformed with pTS22 plasmid harboring yeast Snx3, and the transformants were grown overnight in 2 ml LB medium (with 50 μg/ml kanamycin) at 37°C with shaking. Cells were diluted to an optical density (O.D.) equal to 0.1 in fresh LB medium with 50 μg/ml kanamycin. The culture was then incubated in 37°C incubator until the O.D. reached 0.5. The cultures were then split into two-halves (3 ml each). One tube was used as control, and IPTG (1 mM; Sigma; Cat. No.16758–1G) was added to the other tube. The tubes were incubated at 37°C with shaking for 4 . After 4 h, 1 ml aliquots of cultures from both the tubes were centrifuged at 13 300*g* for 1.5 min. The supernatant was decanted and the cell pellet was resuspended in 20 ml of 2× Lammeli buffer with β-mercaptoethanol and then boiled for 10 min on a 100°C heat block. The boiled samples were then flash chilled on ice and then pulse centrifuged at 13 300*g*, and then samples were subjected to SDS-PAGE. The gel was stained with Coomassie brilliant blue R-250 solution (Biorad; Cat. No. 161–0436) for 1 h, and after destaining images were captured using ChemiDoc-MP (Biorad).

Large scale protein production. The Snx3 construct comprises both a hexa-histidine and T7 tag to facilitate protein purification and immunodetection. The plasmid was transformed into BL21 (DE3) cells and plated onto LB agar plates containing 50 μg/ml kanamycin antibiotic. Transformants were first grown in 5 ml LB-kanamycin culture media overnight at 37°C with constant shaking until O.D. = 4. The cells were diluted to 0.1 O.D. in 100 ml of the same medium, incubated at 37°C with shaking for 6 h until O.D. = 1. The cells were then transferred to a 1 l culture

for ~3 h to reach O.D. between 0.4 and 0.6. IPTG (1 mM) was added and the culture was incubated for 4 h. The cells were harvested by centrifugation in 500 ml centrifuge tubes at 5000*g* at 4°C for 20 min, and the supernatant was discarded. The pellet was resuspended in 30 ml of lysis buffer, and the cells were lysed using a French press. Cell debris was removed by centrifugation at 25 600*g*, 4°C for 20 min. The supernatant was passed over a Ni-NTA agarose column (Invitrogen), which was prequilibrated in 20 mM sodium phosphate buffer, pH 7.4. The column was washed with five column volumes of wash buffer (20 mM sodium phosphate buffer, pH 7.4, 20 mM imidazole) to remove non-specifically bound protein. The washing step was repeated two to three times. Finally, the Snx3 protein was eluted using 25–250 mM gradient of imidazole. Tubes containing the pure recombinant Snx3 were pooled and the purity was checked by SDS-PAGE and western blot. Snx3 protein has a thrombin cleavage site between N-terminal 6 His tag and T7 tag. The His_6 tag was cleaved using thrombin cleancleave™ kit (Sigma, SLBS080V) according to the manufacturer's instructions. After the cleavage, the reaction mixture was passed over the Ni-NTA agarose column to remove the cleaved His tag from the Snx3 protein. Purified Snx3 was mixed with 50% glycerol and stored at –20°C. α-Ssyn was purified following the protocol outlined in reference (87).

PIP strip assay. A protein-lipid overlay assay using PIP strips (Echelon Biosciences; Cat. No. P-6001) was performed to verify that purified recombinant Snx3 binds to PI3P. About 5 μg/ml of recombinant Snx3 was used, and the assay was performed according to the manufacturer instructions.

Preparation of phospholipid vesicles. The lipids 1-palmitoyl-2-oleoyl-sn-glycero-3-phosphocholine (POPC); 1-palmitoyl-2-oleoyl-sn-glycero-3-phospho-L-serine (sodium salt) and 1, 2-dioleoyl-sn-glycero-3-phospho-(1′-myo-inositol-3′-phosphate) (ammonium salt), L-α-phosphatidylinositol and an extruder kit were purchased from Avanti Polar Lipids. Lipids PC, PS, PI and PI3P were dissolved in chloroform at a concentration of 0.1 mg/ml. Solvent was removed by passing a stream of nitrogen gas over the sample, followed by lyophilization. The dried lipid film was then rehydrated with 200 μl of 10 mM HEPES, pH 8.0, 0.1 M NaCl, 1 mM dithiothreitol for 30 min followed by five freeze thaw cycles. The 100 nm homogeneous unilameller vesicles were prepared by passing the lipid solution (up to 20 times) through the extruder with a 0.1 um pore polycarbonate membrane at 10°C above the melting temperature of the lipids. The final concentration of lipids in solution was 500 μM, and the proportion of lipids was 70%:25%:5% [PC:PS:PI (or PI3P)].

Flotation assay (46). Because purified Snx3 strongly adsorbed to the wall of the polypropylene tubes, we tested polycarbonate and cellulose propionate tubes (Beckman Coulter) and found that cellulose propionate adsorbed the least amount of protein compared to the other tubes. Hence, cellulose propionate tubes (Beckman Coulter) was chosen for membrane binding assay. The membrane binding assay were carried out by adding 1 μM of α-synuclein incubated for 4 h followed by the addition of 0.25 μM of Snx3 for 1 h in 25 μl of 500 μM liposomes at 30°C. Each sample was mixed with 55 μl of 60% iodoxanol and loaded into the centrifuge tube. This bottom layer was overlaid with 120 μl of 20% iodoxanol followed by 40 μl of HEPES buffer. The samples were centrifuged at 70 000 rpm in a TLA100 rotor (Beckman Coulter) for 2 h at 4°C. Approximately 4 μl from the top (liposome layer) and bottom (soluble) layers were subjected to SDS-PAGE using 4–20% tris-glycine gels followed by western blotting as described (85).

Cycloheximide assay. Transformed cells were inoculated overnight in 3 ml non-inducing media at starting O.D. of 0.1 and cultured in 30°C incubator. Next day, the culture was centrifuged, washed once with PBS and diluted in 20 ml inducing media (1% galactose) for 6 h and cultured in 30°C incubator. After 6 h, CHX was added to the final concentration of 100 μg/ml. This is referred to as 0 h time-point. The cultures were mixed uniformly and a 1 ml aliquot was immediately transferred to a prelabeled microfuge tube. The rest of the culture was kept for culturing at 30°C. Out of 1 ml aliquot, 200 μl was centrifuged and the cell pellet was used for epifluorescence microscopy. The rest of the aliquot was transferred to pre-chilled microfuge tube on ice containing 20× stop-mix solution (5 mg/ml BSA, 200 mM sodium azide) (88). These steps were repeated for the following time-points at 2 and 4 h. Once all the aliquots were collected and mixed with stop-mix solution, the cells were pelleted, lysed and subjected to SDS-PAGE for western blotting. Experiments (±α-syn) were repeated three times. We measured the Fet3-GFP fluorescence intensity by averaging 50 randomly chosen pixels on the periphery of each cell (100 cells). In total, for the two samples, 1800 cells were counted (2 samples × 900 cells/sample). The person who performed this analysis was blinded as to the identity of the samples.

Statistical analysis. Yeast: P values were determined by a one-way ANOVA with a Bonferroni correction when comparing multiple samples of different treatments to a control. Otherwise, P values were determined by an unpaired, two-tailed Student's *t* test when comparing two samples. Experimental values are means ± SD of typically three independent experiments. Kaleidagraph version 4.5 was used for the statistical tests. Worms: Statistical analyses were performed using one-way ANOVA and a Sidak posthoc analysis ($P < 0.05$) using GraphPad Prism (version 6).

RNA interference (RNAi). The F21D5.3, *fpn1.1*, *smf-3* and *snx-3* RNAi feeding clones and EV clone were purchased from Geneservice. Bacteria expressing these plasmids were isolated and grown overnight in LB media with 100 μg/ml ampicillin. Nematode growth media plates containing 1 μM IPTG were seeded with RNAi feeding clones and allowed to dry. Hermaphrodites at the L4 stage were transferred to RNAi plates and they laid eggs overnight to synchronize the F1 progeny. The dopaminergic neurons in the F1 progeny of the RNAi-treated worms were analyzed for neurodegeneration at days 5 and 7. Two chromosomally integrated transgenic *C. elegans* strains that enable dopaminergic neuron-specific RNAi (72) were utilized. Strain UA196 (*sid-1(pk3321)*; *baIn11*[P*dat-1*::α-syn, P*dat-1*:: GFP]; *baIn33*[P*dat-1*:: *sid-1*, P*myo-2*:: mCherry]), expresses α-syn, GFP, and SID-1 in the dopaminergic neurons and is susceptible to RNAi selectively in this neuronal subset. UA202 (*sid-1(pk3321)*; *vtIs7*[P*dat-1*:: GFP]; *baIn36*[P*dat-1*:: *sid-1*, P*myo-2*:: mCherry]) expresses SID-1 and GFP and acts as a control strain for UA196.

Dopaminergic neurodegeneration analyses in C. elegans. *C. elegans* dopaminergic neurons were analyzed for degeneration as previously described (76). Briefly, strains UA196 and UA202 were treated with F21D5.3, *fpn1.1*, *snx-3*, *smf-3* or EV dsRNA. Nematodes were synchronized, grown at 20°C, and analyzed at days 5 and 7 of development for dopaminergic neurodegeneration. On the day of analysis, the six anterior dopaminergic neurons were examined in 30 adult hermaphrodite worms, in triplicate for each target. Worms were immobilized on glass coverslips using 3 mM levamisole and transferred onto 2% agarose pads on microscope slides. Analysis was performed on a Nikon E800 with an Endow GFP filter cube (Chroma). Worms were considered normal when all six anterior neurons were present without any signs of degeneration (76,89). In total, at

least 90 adult worms were analyzed for each RNAi treatment (30 worms/trial, with a total of 3 trials).

Treatment of C. elegans with the chelator DFO. DFO was purchased from Sigma (St. Louis, MO). DFO was dissolved in water and then added to pre-autoclaved media, with the volume of compound solution taken into account. It was tested in *C. elegans* at a final concentration of 100 μM in water. All 35 mm worm DFO plates were seeded with 100 μl concentrated *E. coli* strain OP50.

Supplementary Material

Supplementary Material is available at *HMG* online.

Acknowledgements

We thank Kelly Tatchell for microscope usage, Chris Patillo and the Feist-Weiller Cancer Center for use of their chemi-doc MP systems, David McGee for his French press and Chris Burd for a plasmid and yeast strains.

Conflict of Interest statement. None declared.

Funding

Supported in part by the Chancellor of LSUHSC-Shreveport, the Department of Biochemistry & Molecular Biology, LSUHSC-Shreveport, and from EPIC.COM [to S.N.W.] and from the Louisiana Biochemical Research Network summer program for undergraduates [to W.O.H and S.N.W.].

References

1. Kalia, L.V. and Lang, A.E. (2015) Parkinson's disease. *Lancet*, **386**, 896–912.
2. Spillantini, M.G., Schmidt, M.L., Lee, V.M., Trojanowski, J.Q., Jakes, R. and Goedert, M. and (1997) Alpha-synuclein in Lewy bodies. *Nature*, **388**, 839–840.
3. Goedert, M., Spillantini, M.G., Del Tredici, K. and Braak, H. (2013) 100 years of Lewy pathology. *Nat. Rev. Neurol.*, **9**, 13–24.
4. Polymeropoulos, M.H., Lavedan, C., Leroy, E., Ide, S.E., Dehejia, A., Dutra, A., Pike, B., Root, H., Rubenstein, J. and Boyer, R. (1997) Mutation in the alpha-synuclein gene identified in families with Parkinson's disease. *Science*, **276**, 2045–2047.
5. Kruger, R., Kuhn, W., Muller, T., Woitalla, D., Graeber, M., Kosel, S., Przuntek, H., Epplen, J.T., Schols, L. and Riess, O. (1998) Ala30Pro mutation in the gene encoding alpha-synuclein in Parkinson's disease. *Nat. Genet.*, **18**, 106–108.
6. Zarranz, J.J., Alegre, J., Gomez-Esteban, J.C., Lezcano, E., Ros, R., Ampuero, I., Vidal, L., Hoenicka, J., Rodriguez, O. and Atares, B. (2004) The new mutation, E46K, of alpha-synuclein causes Parkinson and Lewy body dementia. *Ann. Neurol.*, **55**, 164–173.
7. Proukakis, C., Dudzik, C.G., Brier, T., MacKay, D.S., Cooper, J.M., Millhauser, G.L., Houlden, H. and Schapira, A.H. (2013) A novel alpha-synuclein missense mutation in Parkinson disease. *Neurology*, **80**, 1062–1064.
8. Lesage, S., Anheim, M., Letournel, F., Bousset, L., Honore, A., Rozas, N., Pieri, L., Madiona, K., Duerr, A. and Melki, R. (2013) G51D alpha-Synuclein mutation causes a novel Parkinsonian-pyramidal syndrome. *Ann. Neurol.*, **73**, 459–471.
9. Singleton, A.B., Farrer, M., Johnson, J., Singleton, A., Hague, S., Kachergus, J., Hulihan, M., Peuralinna, T., Dutra, A. and Nussbaum, R. (2003) alpha-synuclein locus triplication causes Parkinson's disease. *Science*, **302**, 841–841.
10. Varkey, J., Mizuno, N., Hegde, B.G., Cheng, N.Q., Steven, A.C. and Langen, R. (2013) alpha-synuclein oligomers with broken helical conformation form lipoprotein nanoparticles. *J. Biol. Chem.*, **288**, 17620–17630.
11. Burre, J., Sharma, M., Tsetsenis, T., Buchman, V., Etherton, M.R. and Sudhof, T.C. (2010) Alpha-synuclein promotes snare-complex assembly in vivo and in vitro. *Science*, **329**, 1663–1667.
12. Scherzer, C.R., Grass, J.A., Liao, Z., Pepivani, I., Zheng, B., Eklund, A.C., Ney, P.A., Ng, J., McGoldrick, M. and Mollenhauer, B. (2008) GATA transcription factors directly regulate the Parkinson's disease-linked gene alpha-synuclein. *Proc. Natl. Acad. Sci. U.S.A.*, **105**, 10907–10912.
13. Dexter, D.T., Wells, F.R., Agid, F., Agid, Y., Lees, A.J., Jenner, P. and Marsden, C.D. (1987) Increased nigral iron content in postmortem parkinsonian brain. *Lancet*, **330**, 1219–1220.
14. Riederer, P., Sofic, E., Rausch, W.D., Schmidt, B., Reynolds, G.P., Jellinger, K. and Youdim, M.B. (1989) Transition metals, ferritin, glutathione, and ascorbic acid in parkinsonian brains. *J. Neurochem.*, **52**, 515–520.
15. Hirsch, E.C., Brandel, J.P., Galle, P., Javoy-Agid, F. and Agid, Y. (1991) Iron and aluminum increase in the substantia nigra of patients with Parkinson's disease: an X-ray microanalysis. *J. Neurochem.*, **56**, 446–451.
16. Temlett, J.A., Landsberg, J.P., Watt, F. and Orime, G.W. (2008) Increased iron in the substantia-nigra compacta of the mptp-lesioned hemiparkinsonian african-green monkey – evidence from proton microprobe elemental microanalysis. *J. Neurochem.*, **62**, 134–146.
17. Oestreicher, E., Sengstock, G.J., Riederer, P., Olanow, C.W., Dunn, A.J. and Arendash, G.W. (1994) Degeneration of nigrostriatal dopaminergic-neurons increases iron within the substantia-nigra – a histochemical and neurochemical study. *Brain Res.*, **660**, 8–18.
18. Glinka, Y., Tipton, K.F. and Youdim, M.B. (1996) Nature of inhibition of mitochondrial respiratory complex I by 6-Hydroxydopamine. *J. Neurochem.*, **66**, 2004–2010.
19. Dauer, W., Kholodilov, N., Vila, M., Trillat, A.-C., Goodchild, R., Larsen, K.E., Staal, R., Tieu, K., Schmitz, Y., Yuan, C.A. *et al.* (2002) Resistance of alpha-synuclein null mice to the parkinsonian neurotoxin MPTP. *Proc. Natl. Acad. Sci. U.S.A.*, **99**, 14524–14529.
20. Youdim, M.B., Stephenson, G. and Ben Shachar, D. (2004) Ironing iron out in Parkinson's disease and other neurodegenerative diseases with iron chelators: a lesson from 6-hydroxydopamine and iron chelators, desferal and VK-28. *Ann. N. Y. Acad. Sci.*, **1012**, 306–325.
21. Yamaguchi-Iwai, Y., Dancis, A. and Klausner, R.D. (1995) AFT1 – a mediator of iron-regulated transcriptional control in *Saccharomyces-cerevisiae*. *EMBO J.*, **14**, 1231–1239.
22. Yamaguchi-Iwai, Y., Stearman, R., Dancis, A. and Klausner, R.D. (1996) Iron-regulated DNA binding by the AFT1 protein controls the iron regulon in yeast. *EMBO J.*, **15**, 3377–3384.
23. Dancis, A., Roman, D.G., Anderson, G.J., Hinnebusch, A.G. and Klausner, R.D. (1992) Ferric reductase of Saccharomyces cerevisiae: molecular characterization, role in iron uptake, and transcriptional control by iron. *Proc. Natl. Acad. Sci. U.S.A.*, **89**, 3869–3873.
24. Martins, L.J., Jensen, L.T., Simon, J.R., Keller, G.L., Winge, D.R. and Simons, J.R. (1998) Metalloregulation of FRE1 and FRE2

homologs in Saccharomyces cerevisiae. *J. Biol. Chem.*, **273**, 23716–23721.
25. Patel, B.N. and David, S. (1997) A novel glycosylphosphatidylinositol-anchored form of ceruloplasmin is expressed by mammalian astrocytes. *J. Biol. Chem.*, **272**, 20185–20190.
26. Strochlic, T.I., Setty, T.G., Sitaram, A. and Burd, C.G. (2007) Grd19/Snx3p functions as a cargo-specic adapter for retromer-dependent endocytic recycling. *J. Cell Biol.*, **177**, 115–125.
27. Strochlic, T.I., Schmiedekamp, B.C., Lee, J., Katzmann, D.J. and Burd, C.G. (2008) Opposing Activities of the Snx3-Retromer complex and ESCRT proteins mediate regulated cargo sorting at a common endosome. *Mol. Biol. Cell*, **19**, 4694–4706.
28. Vilariño-Güell, C., Wider, C., Ross, O.A., Dachsel, J.C., Kachergus, J.M., Lincoln, S.J., Soto-Ortolaza, A.I., Cobb, S.A., Wilhoite, G.J., Bacon, J.A. *et al.* (2011) VPS35 mutations in Parkinson disease. *Am. J. Hum. Genet.*, **89**, 162–167.
29. Zimprich, A., Benet-Pages, A., Struhal, W., Graf, E., Eck, S.H., Offman, M.N., Haubenberger, D., Spielberger, S., Schulte, E.C. and Lichtner, P. (2011) A mutation in VPS35, encoding a subunit of the retromer complex, causes late-onset Parkinson disease. *Am. J. Hum. Genet.*, **89**, 168–175.
30. Lesage, S., Condroyer, C., Klebe, S., Honore, A., Tison, F., Brefel-Courbon, C., Durr, A. and Brice, A. and French Parkinsons Disease Genetics Study Group. (2012) Identification of VPS35 mutations replicated in French families with Parkinson disease. *Neurology*, **78**, 1449–1450.
31. Dhungel, N., Eleuteri, S., Li, L-b., Kramer, N.J., Chartron, J.W., Spencer, B., Kosberg, K., Fields, J.A., Stafa, K., Adame, A. *et al.* (2015) Parkinson's disease genes VPS35 and EIF4G1 interact genetically and converge on alpha-synuclein. *Neuron*, **85**, 76–87.
32. Goncalves, S.A., Macedo, D., Raquel, H., Simoes, P.D., Giorgini, F., Ramalho, J.S., Barral, D.C., Moita, L.F. and Outeiro, T.F. (2016) shRNA-based screen identifies endocytic recycling pathway components that act as genetic modifiers of alpha-synuclein aggregation, secretion and toxicity. *PLoS Genet*, **12**, e100599.
33. Seaman, M.N. (2005) Recycle your receptors with retromer. *Trends Cell Biol.*, **15**, 68–75.
34. Small, S.A. and Petsko, G.A. (2015) Retromer in Alzheimer disease, Parkinson disease and other neurological disorders. *Nat. Rev. Neurosci.*, **16**, 126–132.
35. Williams, E.T., Chen, X. and Moore, D.J. (2017) VPS35, the retromer complex and Parkinson's disease. *J. Parkinson's Dis.*, **7**, 219–233.
36. Haft, C.R., Sierra, M. d l L., Bafford, R., Lesniak, M.A., Barr, V.A. and Taylor, S.I. (2000) Human orthologs of yeast vacuolar protein sorting proteins Vps26, 29, and 35: assembly into multimeric complexes. *Mol. Biol. Cell*, **11**, 4105–4116.
37. Seaman, M.N., McCaffery, J.M. and Emr, S.D. (1998) A membrane coat complex essential for endosome-to-Golgi retrograde transport in yeast. *J. Cell Biol.*, **142**, 665–681.
38. Nothwehr, S.F., Bruinsma, P. and Strawn, L.A. (1999) Distinct domains within Vps35p mediate the retrieval of two different cargo proteins from the yeast prevacuolar/endosomal compartment. *Mol. Biol. Cell*, **10**, 875–890.
39. Seet, L.F. and Hong, W.J. (2006) The Phox (PX) domain proteins and membrane traffic. *Biochim. Biophys. Acta*, **1761**, 878–896.
40. Carlton, J., Bujny, M., Peter, B.J., Oorschot, V.M., Rutherford, A., Mellor, H., Klumperman, J., McMahon, H.T. and Cullen, P.J. (2004) Sorting nexin-1 mediates tubular endosome-to-TGN transport through coincidence sensing of high-curvature membranes and 3-phosphoinositides. *Curr. Biol.*, **14**, 1791–1800.
41. Cullen, P.J. and Korswagen, H.C. (2012) Sorting nexins provide diversity for retromer-dependent trafficking events. *Nat. Cell Biol.*, **14**, 29–37.
42. Askwith, C., Eide, D., Van Ho, A., Bernard, P.S., Li, L., Davis-Kaplan, S., Sipe, D.M. and Kaplan, J. (1994) The FET3 gene of saccharomyces-cerevisiae encodes a multicopper oxidase required for ferrous iron uptake. *Cell*, **76**, 403–410.
43. Dancis, A., Yuan, D.S., Haile, D., Askwith, C., Eide, D., Moehle, C., Kaplan, J. and Klausner, R.D. (1994) Molecular characterization of a copper transport protein in *Saccharomyces-cerevisiae* – an unexpected role for copper in iron transport. *Cell*, **76**, 393–402.
44. Stearman, R., Yuan, D.S., Yamaguchi-Iwai, Y., Klausner, R.D. and Dancis, A. (1996) A permease-oxidase complex involved in high-affinity iron uptake in yeast. *Science*, **271**, 1552–1557.
45. Felice, M.R., De Domenico, I., Li, L.T., Ward, D.M., Bartok, B., Musci, G. and Kaplan, J. (2005) Post-transcriptional regulation of the yeast high affinity iron transport system. *J. Biol. Chem.*, **280**, 22181–22190.
46. Volles, M.J., Lee, S.J., Rochet, J.C., Shtilerman, M.D., Ding, T.T., Kessler, J.C. and Lansbury, P.T. (2001) Vesicle permeabilization by protofibrillar alpha-synuclein: implications for the pathogenesis and treatment of Parkinson's disease. *Biochemistry*, **40**, 7812–7819.
47. Varkey, J., Isas, J.M., Mizuno, N., Jensen, M.B., Bhatia, V.K., Jao, C.C., Petrlova, J., Voss, J.C., Stamou, D.G., Steven, A.C. and Langen, R. (2010) Membrane curvature induction and tubulation are common features of synucleins and apolipoproteins. *J. Biol. Chem.*, **285**, 32486–32493.
48. Peterson, M.R., Burd, C.G. and Emr, S.D. (1999) Vac1p coordinates Rab and phosphatidylinositol 3-kinase signaling in Vps45p-dependent vesicle docking/fusion at the endosome. *Curr. Biol.*, **9**, 159–162.
49. Arlt, H., Auffarth, K., Kurre, R., Lisse, D., Piehler, J. and Ungermann, C. (2015) Spatiotemporal dynamics of membrane remodeling and fusion proteins during endocytic transport. *Mol. Biol. Cell*, **26**, 1357–1370.
50. Jones, E.W., Zubenko, G.S. and Parker, R.R. (1982) PEP4 gene function is required for expression of several vacuolar hydrolases in *Saccharomyces cerevisiae*. *Genetics*, **102**, 665–677.
51. Chen, C.Y., Garcia-Santos, D., Ishikawa, Y., Seguin, A., Li, L.T., Fegan, K.H., Hildick-Smith, G.J., Shah, D.I., Cooney, J.D. and Chen, W. (2013) Snx3 regulates recycling of the transferrin receptor and iron assimilation. *Cell Metabol.*, **17**, 343–352.
52. Tabuchi, M., Yanatori, I., Kawai, Y. and Kishi, F. (2010) Retromer-mediated direct sorting is required for proper endosomal recycling of the mammalian iron transporter DMT1. *J. Cell Sci.*, **123**, 756–766.
53. Lam-Yuk-Tseung, S., Touret, N., Grinstein, S. and Gros, P. (2005) Carboxyl-terminus determinants of the iron transporter DMT1/SLC11A2 isoform II (-IRE/1B) mediate internalization from the plasma membrane into recycling endosomes. *Biochemistry*, **44**, 12149–12159.
54. Lu, L.N., Qian, Z.M., Wu, K.C., Yung, W.H. and Ke, Y. (2017) Expression of iron transporters and pathological hallmarks of Parkinson's and Alzheimer's diseases in the brain of young, adult, and aged rats. *Mol. Neurobiol.*, **54**, 5213–5224.
55. Salazar, J., Mena, N., Hunot, S., Prigent, A., Alvarez-Fischer, D., Arredondo, M., Duyckaerts, C., Sazdovitch, V., Zhao, L.,

Garrick, L.M. *et al*. (2008) Divalent metal transporter 1 (DMT1) contributes to neurodegeneration in animal models of Parkinson's disease. *Proc. Natl. Acad. Sci. U.S.A.*, **105**, 18578–18583.
56. Lucas, M., Gershlick, D.C., Vidaurrazaga, A., Rojas, A.L., Bonifacino, J.S. and Hierro, A. (2016) Structural mechanism for cargo recognition by the retromer complex. *Cell*, **167**, 1623–1635.
57. Harrison, M.S., Hung, C.S., Liu, T.T., Christiano, R., Walther, T.C. and Burd, C.G. (2014) A mechanism for retromer endosomal coat complex assembly with cargo. *Proc. Natl. Acad. Sci. U.S.A.*, **111**, 267–272.
58. Baksi, S., Tripathi, A.K. and Singh, N. (2016) Alpha-synuclein modulates retinal iron homeostasis by facilitating the uptake of transferrin-bound iron: implications for visual manifestations of Parkinson's disease. *Free Radic. Biol. Med.*, **97**, 292–306.
59. Matak, P., Matak, A., Moustafa, S., Aryal, D.K., Benner, E.J., Wetsel, W. and Andrews, N.C. (2016) Disrupted iron homeostasis causes dopaminergic neurodegeneration in mice. *Proc. Natl. Acad. Sci. U.S.A.*, **113**, 3428–3435.
60. McCarthy, R.C., Park, Y.H. and Kosman, D.J. (2014) sAPP modulates iron efflux from brain microvascular endothelial cells by stabilizing the ferrous iron exporter ferroportin. *EMBO Rep.*, **15**, 809–815.
61. Lane, R.F., Raines, S.M., Steele, J.W., Ehrlich, M.E., Lah, J.A., Small, S.A., Tanzi, R.E., Attie, A.D. and Gandy, S. (2010) Diabetes-associated sorcs1 regulates alzheimer's amyloid-beta metabolism: evidence for involvement of sorl1 and the retromer complex. *J. Neurosci.*, **30**, 13110–13115.
62. Gustafsen, C., Glerup, S., Pallesen, L.T., Olsen, D., Andersen, O.M., Nykjaer, A., Madsen, P. and Petersen, C.M. (2013) Sortilin and sorla display distinct roles in processing and trafficking of amyloid precursor protein. *J. Neurosci.*, **33**, 64–71.
63. Ayton, S., Zhang, M., Roberts, B.R., Lam, L.Q., Lind, M., McLean, C., Bush, A.I., Frugier, T., Crack, P.J. and Duce, J.A. (2014) Ceruloplasmin and beta-amyloid precursor protein confer neuroprotection in traumatic brain injury and lower neuronal iron. *Free Radic. Biol. Med.*, **69**, 331–337.
64. Ayton, S., Lei, P., Hare, D.J., Duce, J.A., George, J.L., Adlard, P.A., McLean, C., Rogers, J.T., Cherny, R.A., Finkelstein, D.I. and Bush, A.I. (2015) Parkinson's disease iron deposition caused by nitric oxide-induced loss of beta-amyloid precursor protein. *J. Neurosci.*, **35**, 3591–3597.
65. Lei, P., Ayton, S., Finkelstein, D.I., Spoerri, L., Ciccotosto, G.D., Wright, D.K., Wong, B.X., Adlard, P.A., Cherny, R.A. and Lam, L.Q. (2012) Tau deficiency induces parkinsonism with dementia by impairing APP-mediated iron export. *Nat. Med.*, **18**, 291–295.
66. Hochstrasser, H., Bauer, P., Walter, U., Behnke, S., Spiegel, J., Csoti, I., Zeiler, B., Bornemann, A., Pahnke, J., Becker, G., Riess, O. and Berg, D. (2004) Ceruloplasmin gene variations and substantia nigra hyperechogenicity in Parkinson disease. *Neurology*, **63**, 1912–1917.
67. Hochstrasser, H., Tomiuk, J., Walter, U., Behnke, S., Spiegel, J., Kruger, R., Georg, B., Riess, O. and Berg, D. (2005) Functional relevance of ceruloplasmin mutations in Parkinson's disease. *FASEB J.*, **19**, 1851–1853.
68. Olivieri, S., Conti, A., Iannaccone, S., Cannistraci, C.V., Campanella, A., Barbariga, M., Codazzi, F., Pelizzoni, I., Magnani, G. and Pesca, M. (2011) Ceruloplasmin oxidation, a feature of parkinson's disease csf, inhibits ferroxidase activity and promotes cellular iron retention. *J. Neurosci.*, **31**, 18568–18577.
69. Jin, L.R., Wang, J.A., Zhao, L., Jin, H., Fei, G.Q., Zhang, Y.W., Zeng, M.S. and Zhong, C.J. (2011) Decreased serum ceruloplasmin levels characteristically aggravate nigral iron deposition in Parkinson's disease. *Brain*, **134**, 50–58.
70. Ayton, S., Lei, P., Duce, J.A., Wong, B.X., Sedjahtera, A., Adlard, P.A., Bush, A.I. and Finkelstein, D.I. (2013) Ceruloplasmin dysfunction and therapeutic potential for Parkinson disease. *Ann. Neurol.*, **73**, 554–559.
71. Zhao, N., Xiao, J., Zheng, Z., Fei, G., Zhang, F., Jin, L. and Zhong, C. (2015) Single-nucleotide polymorphisms and haplotypes of non-coding area in the CP gene are correlated with Parkinson's disease. *Neurosci. Bull.*, **31**, 245–256.
72. Harrington, A.J., Yacoubian, T.A., Slone, S.R., Caldwell, K.A. and Caldwell, G.A. (2012) Functional analysis of VPS41-mediated neuroprotection in *Caenorhabditis elegans* and mammalian models of Parkinson's disease. *J. Neurosci.*, **32**, 2142–2153.
73. Usenovic, M., Knight, A.L., Ray, A., Wong, V., Brown, K.R., Caldwell, G.A., Caldwell, K.A., Stagljar, I. and Krainc, D. (2012) Identification of novel ATP13A2 interactors and their role in alpha-synuclein misfolding and toxicity. *Hum. Mol. Genet.*, **21**, 3785–3794.
74. Calixto, A., Chelur, D., Topalidou, I., Chen, X.Y. and Chalfie, M. (2010) Enhanced neuronal RNAi in C. elegans using SID-1. *Nat. Method*, **7**, 554–559.
75. Cao, S., Hewett, J.W., Yokoi, F., Lu, J., Buckley, A.C., Burdette, A.J., Chen, P., Nery, F.C., Li, Y., Breakefield, X.O. *et al*. (2010) Chemical enhancement of torsinA function in cell and animal models of torsion dystonia. *Dis. Mod. Mech.*, **3**, 386–396.
76. Hamamichi, S., Rivas, R.N., Knight, A.L., Cao, S., Caldwell, K.A. and Caldwell, G.A. (2008) Hypothesis-based RNAi screening identifies neuroprotective genes in a Parkinson's disease model. *Proc. Natl. Acad. Sci. U.S.A.*, **105**, 728–733.
77. Ziegler, L., Terzulli, A., Sedlak, E. and Kosman, D.J. (2010) Core glycan in the yeast multicopper ferroxidase, Fet3p: a case study of N-linked glycosylation, protein maturation, and stability. *Prot. Sci.*, **19**, 1739–1750.
78. Ke, Y., Chang, Y.Z., Duan, X.L., Du, J.R., Zhu, L., Wang, K., Yang, X.D., Ho, K.P. and Qian, Z.M. (2005) Age-dependent and iron-independent expression of two mRNA isoforms of divalent metal transporter 1 in rat brain. *Neurobiol. Aging*, **26**, 739–748.
79. Roth, J.A., Singleton, S., Feng, J., Garrick, M. and Paradkar, P.N. (2010) Parkin regulates metal transport via proteasomal degradation of the 1B isoforms of divalent metal transporter 1. *J. Neurochem.*, **113**, 454–464.
80. Snyder, H., Mensah, K., Theisler, C., Lee, J., Matouschek, A. and Wolozin, B. (2003) Aggregated and monomeric alpha-synuclein bind to the S6' proteasomal protein and inhibit proteasomal function. *J. Biol. Chem.*, **278**, 11753–11759.
81. Follett, J., Bugarcic, A., Yang, Z., Ariotti, N., Norwood, S.J., Collins, B.M., Parton, R.G. and Teasdale, R.D. (2016) Parkinson disease-linked Vps35 R524W mutation impairs the endosomal association of retromer and induces alpha-synuclein aggregation. *J. Biol. Chem.*, **291**, 18283–18298.
82. Qiao, L., Hamamichi, S., Caldwell, K.A., Caldwell, G.A., Yacoubian, T.A., Wilson, S., Xie, Z.L., Speake, L.D., Parks, R., Crabtree, D. *et al*. (2008) Lysosomal enzyme cathepsin D protects against alpha-synuclein aggregation and toxicity. *Mol. Brain*, **1**, 17.
83. Harterink, M., Port, F., Lorenowicz, M.J., McGough, I.J., Silhankova, M., Betist, M.C., van Weering, J.R.T., van Heesbeen, R., Middelkoop, T.C., Basler, K. *et al*. (2011) A SNX3-dependent retromer pathway mediates retrograde transport of the Wnt sorting receptor Wntless and is required for Wnt secretion. *Nat. Cell Biol.*, **13**, 914–923.

84. Burke, D., Dawson, D. and Stearns, T. (2000) *Methods in Yeast Genetics*. Cold Spring Harbor Lab Press, Cold Spring Harbor, NY.
85. Flower, T.R., Chesnokova, L.S., Froelich, C.A., Dixon, C. and Witt, S.N. (2005) Heat shock prevents alpha-synuclein-induced apoptosis in a yeast model of Parkinson's disease. *J. Mol. Biol.*, **351**, 1081–1100.
86. Gassmann, M., Grenacher, B., Rohde, B. and Vogel, J. (2009) Quantifying western blots: pitfalls of densitometry. *Electrophoresis*, **30**, 1845–1855.
87. Silva, B.A., Einarsdóttir, O., Fink, A.L. and Uversky, V.N. (2013) Biophysical characterization of α-synuclein and rotenone interaction. *Biomolecules*, **3**, 703–732.
88. Buchanan, B.W., Lloyd, M.E., Engle, S.M. and Rubenstein, E.M. (2016) Cycloheximide chase analysis of protein degradation in *Saccharomyces cerevisiae*. *J. Vis. Exp.*, **110**, e53975.
89. Cao, S.S., Gelwix, C.C., Caldwell, K.A. and Caldwell, G.A. (2005) Torsin-mediated protection from cellular stress in the dopaminergic neurons of *Caenorhabditis elegans*. *J. Neurosci.*, **25**, 3801–3812.
90. Lee, Y.J., Wang, S., Slone, S.R., Yacoubian, T.A. and Witt, S.N. (2011) Defects in very long chain fatty acid synthesis enhance alpha-synuclein toxicity in a yeast model of Parkinson's disease. *PLoS One*, **6**, e15946.